People's Democratic Republic of Algeria
Ministry of Higher Education and Scientific Research

University of Batna 2 – Mostefa Ben Boulaïd
Faculty of Technology
Department of Electronics

Dissertation

Presented in fulfillment of the requirement of the degree of
Doctor of Science in Electronics
Option: Microelectronics

Entitled:

Theoretical investigation of phosphorene for nanoelectronic applications

Presented by:

FARAH Seyf El Islam

Committee members:

Dr. Ramdane MAHAMDI	Prof.	University of Batna 2	Chairman
Dr. Zohir DIBI	Prof.	University of Batna 2	Advisor
Dr. AbdELALI SAOULI	M.C.A	University of Constantine 1	Examiner
Dr. AbdELAZIZ RABEHI	M.C.A	University of Djelfa	Examiner
Dr. Fayçal DJEFFAL	Prof.	University of Batna 2	Invited

May 2023

DEDICATION

This dissertation is dedicated to my lovely Mother, my

brothers, and my sister

Acknowledgments

First of all, I am deeply grateful to **The Almighty Allah (SWT)**, the Most High, the Most Compassionate, and the Most Merciful for all his giving, and for the opportunity He gave me to study, to research and to write and finalizing this Ph.D. project. I Thank **Allah (SWT)**, my outmost thanks, for providing me this opportunity and granting me the capability to proceed successfully.

I must acknowledge my advisor **Professor Zohir DIBI**, the person to whom I wish to convey my solidest gratitude and profound respect. His friendly mentorship and wholehearted guidance have been tremendously helpful.

I would like to thank **Ramdane MAHAMDI** from University of Batna-2- for being president of the examination committee. I thank **Professor Fayçal DJEFFAL** from University of Batna 2, for being invited member. And I thank my oral thesis committee members, **M.C.A AbdELALI SAOULI** from University of Constantine 1, and **M.C.A AbdELAZIZ RABEHI** from University of Djelfa, for accepting, taking time to serve as committee members, to review this dissertation and to give valuable comments.

I am really grateful to **Professor Fayçal DJEFFAL**, and my colleague **Dr. Hichem FERHATI** for their valuable remarks. Their friendly and wholehearted opinions have been highly helpful.

Finally, I would like to take this opportunity to thank **all** my friends and colleagues and the staff at the Department of

Electronics, University of Batna -2- who have given their support and helped me in completing this work.

If I did not mention someone's name here, it does not mean that I do not acknowledge your support and help. Again, I would like to thank everyone who supported and helped me during my Ph.D. study.

FARAH SEYF EL ISLAM

Abstract

In this work we present a new broadband mid-Infrared (mid-IR) InGaZnO (IGZO) thin-film phototransistor (TF PT) based on both Black Phosphorus (BP) capping layer incorporating gold (Au) intermediate ultrathin-film. The electronic and optical properties of bulk BP are carried out using density functional theory (DFT) computations, including Perdew-Burke-Ernzerhof Generalized Gradient Approximation (PBE-GGA) and the screened hybrid (YS-PBE0) functionals with van der Waals correction. It is found that BP exhibits interesting performances for mid-IR optoelectronic applications, at room temperature. To enhance the absorption of the BP material for broadband mid-IR spectrum, a new strategy is proposed by optimizing the sensitive layer using finite-difference time-domain (FDTD) modeling and particle swarm optimization (PSO) approaches. The photoresponse properties of the optimized broadband mid-IR IGZO TF PT with BP/Au/BP capping layer are carefully analyzed. It is found that the proposed device shows high photodetection performances with a high current ratio exceeding 180 dB over a wide voltage window. Besides, it is revealed that the introduced ultrathin Au layer within BP enhances the absorbance capability over the mid-IR spectrum, which significantly improves the performance of the broadband mid-IR sensor. Therefore, the proposed approach based on combining DFT analysis with FDTD simulation supported by PSO optimization opens up a new strategy for the development of high-performance optoelectronic devices.

In second part, a new high-performance broadband Infrared Optically Controlled Graphene Field-Effect Transistor (IR–OC–GFET) using strained black phosphorus sensing gate is proposed and investigated. The impact of the hydrostatic pressure on the optoelectronic properties of bulk Black Phosphorus (BP) is studied using density functional theory (DFT) calculations, including Perdew-Burke-Ernzerhof Generalized Gradient Approximation (PBE-GGA) and the screened hybrid (YS-PBE0) function with van der Waals correction. It is revealed that the electronic and the optical properties of BP were substantially affected by the pressure effects, where the band gap energy decreases with increasing the hydrostatic pressure. The phototransistor drain current is calculated by self-consistently solving the Schrödinger/Poisson equations based on Non-Equilibrium Green's function (*NEGF*) approach. The impact of strained BP sensing gate material on the device sensing properties is investigated. It is found that the proposed device with strained sensing gate provides enhanced optical performances over the middle infrared (Mid-IR) spectral band, making it a new potential alternative photoreceiver for chip-level optical communications.

Keywords: 2D; Black phosphorus, Phosphorene, Graphene; DFT, Van der Waals correction; DFTD3, PSO, FDTD; phototransistor; Optical properties; Electronic properties; InGaZnO.

Résumé

Dans ce travail, nous présentons un nouveau phototransistor infrarouge à large bande InGaZnO (IGZO), et à couche mince (TF PT), basé sur une couche de Revêtement en phosphore noir (BP) incorporant un film ultra-mince intermédiaire en or (Au). Les propriétés électroniques et optiques de Phosphorene sont obtenues en utilisant la théorie de la fonctionnelle de la densité (DFT), y compris l'approximation généralisée du gradient de Perdew-Burke-Ernzerhof (PBE-GGA) et les fonctionnelles hybrides criblées (YS-PBE0) avec la correction de van der Waals. On constate que le Phosphorene présente des performances intéressantes pour les applications optoélectroniques dans la plage IR moyen, à la température ambiante. Pour améliorer l'absorption du matériau Phosphorene dans la plage infrarouge moyen à large bande, une nouvelle stratégie est proposée en optimisant la couche sensible à l'aide de la méthode de modélisation dans le domaine temporel à différence finie (FDTD) et l'optimisation par essaims particulaires (PSO). Les propriétés de photoréponse de l'IGZO TF PT IR-moyen à large bande optimisé avec une couche de Revêtement BP/Au/BP sont analysées. On constate que le dispositif proposé présente des performances de photodétection élevées avec un rapport de courant élevé dépassant 180 dB. En outre, il est révélé que la couche Au ultra-mince introduite dans le Phosphore

noir améliore la capacité d'absorption dans le domaine IR moyen, ce qui améliore considérablement les performances du capteur infrarouge à large bande. Par conséquent, l'approche proposée basée sur la combinaison de l'analyse DFT avec la simulation FDTD soutenue par l'optimisation PSO ouvre des nouvelles perspectives pour le développement de dispositifs optoélectroniques à hautes performances.

En deuxième partie; un nouveau transistor à effet de champ à base de graphène contrôlé optiquement par l'infrarouge (IR-OC-GFET) à large bande et à haute performance, utilisant une grille de détection forcée à base de phosphore noir, est proposé et étudié. L'impact de la pression hydrostatique sur les propriétés optoélectroniques du phosphorene est étudié à l'aide de la théorie de la fonctionnelle de la densité (DFT), comprenant l'approximation de gradient généralisée de Perdew-Burke-Ernzerhof (PBE-GGA) et la fonction hybride projetée (YS-PBE0) avec la correction de van der Waals. A travers ce travail, il s'avère que les propriétés électroniques et optiques du phosphorene ont été considérablement affectées par les effets de la pression, l'énergie de la bande interdite dimine avec l'augmentation de la pression hydrostatique. Le courant de drain du phototransistor est calculé de manière autoconsistante en résolvant les équations de Schrödinger/Poisson basées sur l'approche de la fonction non-équilibre de Green's (NEGF). L'impact du matériau de la grille de détection forcée à base de phosphorene sur les propriétés de détection du dispositif est étudié. Il s'avère que le dispositif proposé avec une grille de détection forcée offre des performances optiques améliorées par rapport à celle à bande spectrale de l'infrarouge moyen (Mid-IR), ce qui donne un nouveau photorécepteur à utiliser sur puce électronique pour le domaine des commincations optiques.

Keywords: Matériau bidimensionnel; Phosphore noir, Phosphorène, Graphène; Théorie de la fonctionnelle de la densité, Équation d'état de van der Waals; DFTD3, PSO, FDTD; phototransistor; Propriétés optiques; Propriétés électroniques; InGaZnO.

ملخص

في هذا العمل تم اقتراح والتحقق من ترانزستور جديد من الجرافين عالي الأداء و عريض النطاق للأشعة تحت الحمراء ذات التحكم البصري باستخدام قاعدة استشعار من الفوسفور الأسود المتوتر. و تم دراسة تأثير الضغط الهيدروستاتيكي على الخصائص الإلكترونية و الضوئية للفوسفور الأسود باستخدام نظرية الكثافة الوظيفية بما في ذلك تقريب التدرج المعمم والدالة الهجينة مع تصحيح فان دير فالس.

تم أيضا الكشف عن أن الخواص الإلكترونية والبصرية للفوسفور الأسود قد تأثرت بشكل كبير بتغيرات الضغط ، حيث تنخفض طاقة فجوة النطاق مع زيادة الضغط الهيدروستاتيكي. و بناءا على أنه يتم حساب تيار باعث الترانزستور الضوئي عن طريق حل معادلات شرودينجر و بواسون بشكل ثابت بناءً على نهج دالة غرينز غير المتوازنة، تم التحقق من تأثير قاعدة الاستشعار من الفوسفور الأسود المتوتر على خصائص استشعار الجهاز. و وجد أن الجهاز المقترح مع قاعدة استشعار متوترة من الفوسفور الأسود توفر أداء بصريًا محسنًا على نطاق الطيف المتوسط ذوالأشعة تحت الحمراء, مما يجعله جهاز استقبال ضوئي بديل محتمل جديد للاتصالات البصرية على مستوى الرقائق.

الكلمات المفتاحية مادة ثنائية الأبعاد، الفوسفور الأسود، الفوسفورين، الغرافين، نظرية الكثافة الوظيفية، معادلة فان دير فالس، الترانزستور الضوئي، الخصائص الإلكترونية، الخواص البصرية.
InGaZnO, DFTD3, PSO, FDTD.

Table of Contents

Chapter II: Density functional theory

Chapter III: A novel broadband mid infrared phototransistor using BP capping layer

Chapter IV: Broadband Mid-IR graphene-phototransistor using strained black phosphorus sensing gate

Conclusion

List of Figures

List of Tables

Introduction

1. Introduction

Over the past ten years, two-dimensional (2D) and quasi-2D materials has received a huge interest, started when graphene and graphene oxide were more widely recognized in science. In this context, there has been a lot of scientific interest in 2D materials, technology relating to semiconductors has advanced significantly [1, 2, 3]. The intriguing and incredibly uncommon physical, chemical, and material features of graphene which is a single sheet of graphite, sparked this interest. The anisotropy and atomic thickness of the graphene sheet are the main sources of many of these features. Graphene has been emerged for the design of various high-performance nanoelectronic and optoelectronic devices, showing a great potential for outperforming the conventional ones. These interesting properties paved the way for the discovery of several mono-layer materials such as silicene, germanene, phosphorene,…etc [4, 5, 6, 7]. Particularly, phosphorene was recently rediscovered from the perspective of a 2D layered material, 100 years after its first successful synthesis in the bulk form in 1914[8, 9]. Lately, Black phosphorus (BP) is another elemental layered substance that has reemerged. Like graphite, BP is a layered material with a single element that is readily exfoliated to few layer or single structures [10, 11]. There are multiple polytypes of phosphorus that can be divided into three allotropes: white, red, and black. Van der Waals interactions link covalent structural motifs throughout a range of molecular forms, including low-dimensional molecules (0D, white phosphorus), polymer structures (1D, phosphorus nanorods), layered (2D, BP), and tubular structures (2D and 3D, crystalline forms of red phosphorus) [12, 13]. Accordingly, layered BP is the least poisonous and reactive form of phosphorus and is stable thermodynamically at ambient temperature [14, 15, 16]. Despite the complex fabrication process of BP, it shows a high carrier mobility of 1000 $cm^2\ V^{-1}\ s^{-1}$ at ambient temperature, a band gap of 0.3 eV (in bulk form), and a highly anisotropic layered structure that allows compound intercalation [17, 18, 19]. A single sheet of BP, or phosphorene, is made up of parallel puckered double layers with three covalent bonds between each phosphorus atom and no double bonds in the structure. This is in contrast to graphene, which is made up of individual carbon atoms bonded to their three neighbors in a form resembling a honeycomb. Much like graphite, multi-layer phosphorene sheets are pinned vertically and kept together by weak van der Waals interactions between layers.

Because of its fascinating electrical and optical characteristics, including an extremely narrow band gap, tunable mid-IR photoresponse, and high charge carrier mobility, black phosphorus (BP) has recently piqued the interest of researchers working on a wide range of optoelectronic applications [20]. Due to these benefits, the BP material could be a viable substitute for optical sensing in broadband IR optoelectronic and IR optical interconnection applications, bridging the gap between the near and far infrared sensing bands. Furthermore, the BP thin-film surface lack of dangling bonds helps to prevent lattice mismatch problems, which makes it dependable and compatible with CMOS processing technologies [21]. In this context, various IR photosensors based on BP building block have been proposed and investigated, showing a great promise in achieving good photoresponse characteristics [22]. However, their high noise effects and limited sensitive band constitute their major challenges, for the emerging IR optoelectronic systems. Despite the exciting optical and electrical characteristics that the BP demonstrated, more work needs to be done on BP-based photosensors in order to enhance their functionality and enlarge their wavelength range of detection (far and middle IR). Stated differently, BP-based optoelectronic research is still in its early stages and requires improvements to the BP thin-film total absorbance over the infrared spectral region, which is currently relatively low. Thus, in order to improve the optical performances of BP thin-film for broadband infrared photodetection applications, new strategies and design methodologies are still required for the potential improvement of the emerging IR sensors.

2. Dissertation outline

This thesis describes two IR sensors based on monolithic photonic platforms to solve the above mention trade-offs. The primary component used to develop new phototransistors and optoelectronic device models is black phosphorus. To do so, Density functional theory (DFT) methods are used to determine the electrical and optical characteristics of BP. The electronic structure of molecules, atoms, and solids can be successfully calculated using DFT. The quantitative comprehension of material properties from the foundational principles of quantum mechanics is its aim. In this dissertation, we firstly using accurate DFT computation within PBE-GGA and screened hybrid YS-PBE0 functional while accounting for van der Waals correction, to investigate electrical and optical characteristics of bulk BP. The first contribution relies on proposing a novel broadband Infrared IGZO thin-film phototransistor (TF PT). The

second contribution of the thesis consists of using strained BP IR-sensitive material with graphene channel to develop a novel highly sensitive broadband Mid-IR phototransistor device.

This dissertation is organized into four chapters that provide an overview of the research that was done. In first chapter, we will briefly discuss applications of 2D black phosphorus material and their recent progress. To beginning, with defining black phosphorus, and we will provide an overview of their potential applications. Next, we discuss their recent progress, their advantages and disadvantages, and future challenges also are presented. This chapter can be viewed as a foundational piece for subsequent chapters.

The second chapter aims to provide an overview of DFT by outlining the theoretical underpinnings, popular approximations, current advancements, challenges addressed, and potential future directions. Quantum-mechanical (QM) techniques like DFT are utilized in physics and chemistry to determine the electronic structure of atoms, solids, and molecules. Its goal is the quantitative understanding of material properties from the fundamental laws of quantum mechanics. DFT is a low-cost, quick QM theory that is used to precisely calculate a number of solids physical properties. The Hohenberg-Kohn and Kohn-Sham theorems, which form the basis of density-functional theory, are expanded from their original formulation to include a wide range of physical circumstance.

In chapter three, the electronic and optical properties of bulk BP are investigated using accurate DFT computation within PBE-GGA and screened hybrid YS-PBE0 functional taking into consideration van der Waals correction. Moreover, a new broadband Infrared IGZO TF PT based on optimized BP/Au/BP sensitive film is proposed and analyzed by developing DFT-FDTD numerical models combined with a PSO-based optimization technique. Using this new systematic investigation, the proposed approach offers exciting opportunities for designing high-performance mid-IR broadband optoelectronic devices.

The main objective of the last chapter is to exploit the high-performance properties of graphene and strained BP materials in order to develop an efficient broadband Mid-IR phototransistor. The drain current is calculated by solving the Schrödinger equation using non-equilibrium Green's function (NEGF) formalism self-consistently coupled with 2D-Poisson equation. The role of strained BP sensing gate in enhancing the

broadband IR OC-GFET performance is demonstrated. Therefore, combining strained BP sensing gate with graphene-channel material offers exciting opportunities for designing high-performance mid-IR broadband optoelectronic devices.

References

[1] El-Bakkali. A, Sadki. S, Drissi. L. B, & Djeffal. F, Layers engineering optoelectronic properties of 2D hexagonal GeS materials, Physica E: Low-dimensional Systems and Nanostructures, 133(2021), 114791.

[2] Drissi. L.B, Kanga. N.B.-J, Lounis. S, Djeffal. F, Haddad. S, Electron-phonon dynamics in 2D carbon based-hybrids XC (X = Si, Ge, Sn), Journal of Physics Condensed Matter 31(13),135702, 2019.

[3] L. B. Drissi, F. Z. Ramadan, H. Ferhati, F. Djeffal and N. B.-J. Kanga, New highly efficient 2D SiC UV-absorbing material with plasmonic light trapping, Journal of Physics Condensed Matter vol. 32, pp. 025701, 2020.

[4] S.E. Farah, H. Ferhati, Z. Dibi, F. Djeffal, Performance analysis of broadband Mid-IR graphene-phototransistor using strained black phosphorus sensing gate: DFT-NEGF investigation, Micro and Nanostructures, 163 (2022), Article 107187.

[5] Kadri. A, Ferhati. H, & Djeffal. F, Giant responsivity of a new optically controlled graphene UV-phototransistor using graded band-gap ZnMgO gate. Sensors and Actuators A: Physical, 325, 112701, 2021.

[6] H. Ferhati and F. Djeffal, Performance assessment of Gr/Si/Gr UV-photodetector: Design and optimization of graphene interdigitated electrodes, Superlattices and Microstructures 132, 106166, 2019.

[7] M. Kadri, F. Djeffal, H. Ferhati, Performance analysis of a new graphene basedphototransistor for ultra-sensitive infrared sensing applications, Optik 176, 24-31, 2019.

[8] Aijun. Yang , Dawei. Wang, Xiaohua. Wang, Dongzhi. Zhang, Nikhil. Koratkar, Mingzhe. Rong, “Recent advances in phosphorene as a sensing material,” nano today, vol. 20, pp. 13-32, 2018.

[9] W.L. Lu, H.Y. Nan, J.H. Hong, Y.M. Chen, C. Zhu, Z. Liang, X.Y. Ma, Z.H. Ni, C.H. Jin, Z. Zhang, “Plasma-assisted fabrication of monolayer phosphorene and its Raman characterization,” Nano Res, vol. 7, pp. 853–859, 2014.

[10] A.H. Woomer, T.W. Farnsworth, J. Hu, R.A. Wells, C.L. Donley, S.C. Warren, “Phosphorene: Synthesis, Scale-Up, and Quantitative Optical Spectroscopy,” ACS Nano, vol. 9, pp. 8869–8884, 2015.

[11] Ling. Xi, Wang. Han, Huang. Shengxi, Xia. Fengnian, Dresselhaus. Mildred. S, “The renaissance of black phosphorus,” Proceedings of the National Academy of Sciences. Vol. 112, pp. 4523–4530, 2015.

[12] R. Gusmao, Z. Sofer, M. Pumera, “Black Phosphorus Rediscovered: From Bulk to Monolayer,” Angewandte Chemie International, vol. 56, pp. 8052-8072, 2017.

[13] J. Zhu, H. Park, J. Chen, X. Gu, H. Zhang, S. Karthikeyan, N. Wendel, S. A. Campbell, M. Dawber, X. Du M. Li, J.-P. Wang, R. Yang, X. Wang, “Revealing the Origins of 3D Anisotropic Thermal Conductivities of Black Phosphorus,” Adv. Electron. Mater, vol. 2, pp. 1600040, 2016.

[14] A. Favron, E. Gaufrès, F. Fossard, A.-L. Phaneuf-L'Heureux, N. Y.- W. Tang, P. L. Lévesque, A. Loiseau, R. Leonelli, S. Francoeur, R. Martel, "Exfoliating pristine black phosphorus down to the monolayer: photo-oxidation and electronic confinement effects," Cond. Mater, vol. 1, pp.1408.0345, 2015.

[15] X. Liu, J. D. Wood, K. S. Chen, E. Cho, M. C. Hersam, "Thermal Decomposition of Exfoliated Two-Dimensional Black Phosphorus," J. Phys. Chem. Lett, vol. 6, pp. 773–778, 2015.

[16] A. Castellanos-Gomez, L. Vicarelli, E. Prada, J. O. Island, K. L. Narasimha-Acharya, S. I. Blanter, D. J. Groenendijk, M. Buscema, G. a. Steele, J. V. Alvarez, H. W. Zandbergen, J. J. Palacios, H.S.J. van der Zant, "Isolation and charachterization of few-layer black phosphorus," 2D Mater, vol. 1, pp. 25001, 2014.

[17] J. Qiao, X. Kong, Z.-X. Hu, F. Yang, W. Ji, "High-mobility transport anisotropy and linear dichroism in few-layer black phosphorus," Nat. Commun, vol. 5, an. 4475, 2014.

[18] X. Li, B. Deng, X. Wang, S. Chen, M. Vaisman, S. Karato, G. Pan, M. L. Lee, J. Cha, H. Wang F. Xia, "Synthesis of thin-film black phosphorus on a flexible substrate," 2D Mater, vol. 2, pp. 31002, 2015.

[19] L. Li, Y. Yu, G. J. Ye, Q. Ge, X. Ou, H. Wu, D. Feng, X. H. Chen, Y. Zhang, "Black phosphorus field-effect transistors," Nat. Nanotechnol, vol.9, pp. 372–377, 2014.

[20] Q. Liu, X. Zhang, L. B. Abdalla, A. Fazzio, A. Zunger, "Switching a Normal Insulator into a Topological Insulator via Electric Field with Application to Phosphorene," Nano Lett, vol. 15, pp. 1222–1228, 2015.

[21] F.Djeffal, M. Chahdi, A. Benhaya, M.L.Hafiane, An approach based on neural computation to simulate the nanoscale CMOS circuits: Application to the simulation of CMOS inverter, Solid-State Electronics, pp.26-34, 51 (1), 2007.

[22] Ferhati, H., Djeffal, F., & Drissi, L. B. Enhanced infrared photoresponse of a new InGaZnO TFT based on Ge capping layer and high-k dielectric material. Superlattices and Microstructures, 106967, 2021.

Chapter I

Phosphorene Applications: Recent Progress

Abstract: *This chapter provides a summary of the core ideas related to BP and phosphorene. At the beginning, we define its structures and synthesises methods, and we give a detailed description of their advantages and properties. Then we elucidate and describe their applications. A literature review very detailed on the recent progress and future challenges is at last presented.*

I.1. Chapter overview

In the current era of nanotechnology the discovery of graphene has paved the way for the investigation and creation of numerous innovative two-dimensional materials. The distinct physical and chemical characteristics of two-dimensional materials have facilitated research and elevated them above commercial 2D materials utilized in many applications. It is anticipated that extensive study into 2D materials will produce new materials with improved qualities that will be advantageous to both business and society at large. Graphene is regarded as the fundamental material for the development of two-dimensional materials, such as hexagonal boron nitride (h-BN), transition metal dichalcogenides (TMDs, such as MoS_2), and black phosphorous or phosphorene [1]. One century after its first successful synthesis in the bulk form in 1914, phosphorene was recently rediscovered from the perspective of a 2D layered material. 2D materials have been triggering intensive research interest. Much progress has been made in semiconductor technology. In this chapter, we will briefly discuss applications of 2D black phosphorus material and their recent progress. To beginning, with defining black phosphorus and phosphorene, and we will give a global description of their applications. Then we will describe their recent progress. Their advantages and disadvantages and future challenges are also presented. This chapter can be considered as an introductory platform for further chapters.

I.2. Allotropes of phosphorus

Elemental phosphorus can exist in a large number of allotropes, the most common of which are white and red solids. Solid violet and black allotropes are also recognized. The gaseous phosphorus exists as diphosphorus and atomic phosphorus.

I.3. Black phosphorus

At room temperature and pressure, black phosphorus is the thermodynamically stable form of phosphorus, with a heat of figuration of −39.3 kJ/mol (relative to white phosphorus which is defined as the standard state) [2]. It was first synthesized via heating white phosphorus under high pressures (12,000 atmospheres) in 1914. As a 2D material, in semblance, properties, and structure, black phosphorus is very much like graphite with both being black and flaky, a conductor of electricity, and having puckered sheets of related atoms. Black phosphorus has an orthorhombic pleated

honeycomb structure and is the lower reactive allotrope, a result of its lattice of interlinked six-membered rings where each atom is bonded to three other atoms. In this structure, each phosphorus atom has five outer shell electrons. Black phosphorus can also take a cubic crystal lattice structure. In 1914, the Nobel prize winner Percy Williams Bridgman made the first high-pressure synthesis of black phosphorus crystals. Metal salts stimulate the synthesis of black phosphorus [2].

Figure I.1: Black phosphorus crystals in a closed ampoule.

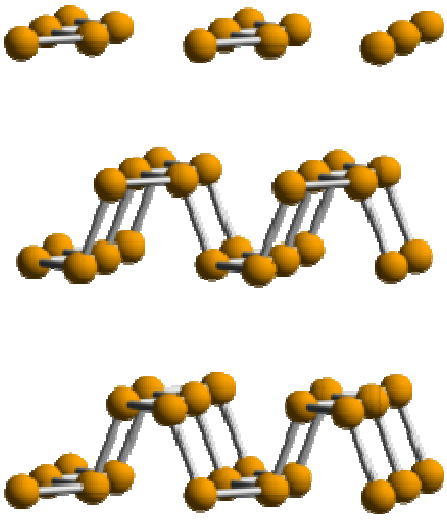

Figure I.2: a black phosphorus unit cell (orthorhombic) with Cmca space group.

I.4. Phosphorene

In general, the preparation of 2D materials can be classified into two approaches, namely top-down methods and bottom-up methods. The most two common top-down methods are mechanical exfoliation and liquid exfoliation, and have been

widely used to prepare 2D materials including phosphorene. Chemical vapor deposition (CVD) is the most common bottom up method and has been successfully adopted to obtain various 2D materials, including graphene , $MoSe_2$, ReS_2, etc. Regrettably, CVD fabrication is almost totally truant at present for phosphorene, due to the low chemical stability of phosphorene. This prevents the growth of large-area and uniform phosphorene and its workable applications.

- **Mechanical exfoliation**

Also known as "the scotch-tape method", mechanical exfoliation is managed with a scotch tape to peel nanoflakes of bulk crystals. A wide range of 2D nanosheets has made by using this method.The scotch-tape method is simple and cheap, and prepares crystal samples with very high quality, mechanical exfoliation procured flakes to study the fundamental properties and possible applications of 2D materials. IN 1914, by using Scotch-tape method, phosphorene was made from bulk BP [3].

In spite of the high purity and neatness of phosphorene prepared by mechanical cleavage, this method have some defects. Espicially in time-consuming and labor intensive . Besides, it is intrinsically unscalable and lack of systematic control of shape, size and thickness, as has limited its use to lab scale fundamental studies. A further disadvantage is the residual organic contamination resulted from the adhesive tapes.

What's more, the mechanically exfoliated phosphorene experienced significant irreversible disintegration when exposed to ambient conditions.

Considering these issues, Gomez et al [3]. sophisticated a modified mechanical exfoliation method by using an intermediate viscoelastic and acquired higher production yield than conventional mechanical exfoliation with smaller contamination. Lu et al [3]. successfully isolated mono-layer phosphorene (Fig.I.3a) through a novel approach by mechanical exfoliation combined with a subsequent Ar+ plasma thinning process. The BP nanosheets granted by this technique are not only controllable and homogeneous (Fig.I.3b) but also highly crystalline. The plasma-assisted thickness control of BP flakes was also proved by Jia et al. and Lee et al [3].

➢ **Liquid phase exfoliation**

Liquid phase exfoliation (LPE) is an operation where layered materials are exfoliated from bulk crystal and colloidal scuttles are created in the solution. A large-scale production of 2D nanomaterials in solution are provided by This approach with a low cost, simple and efficient method [3].

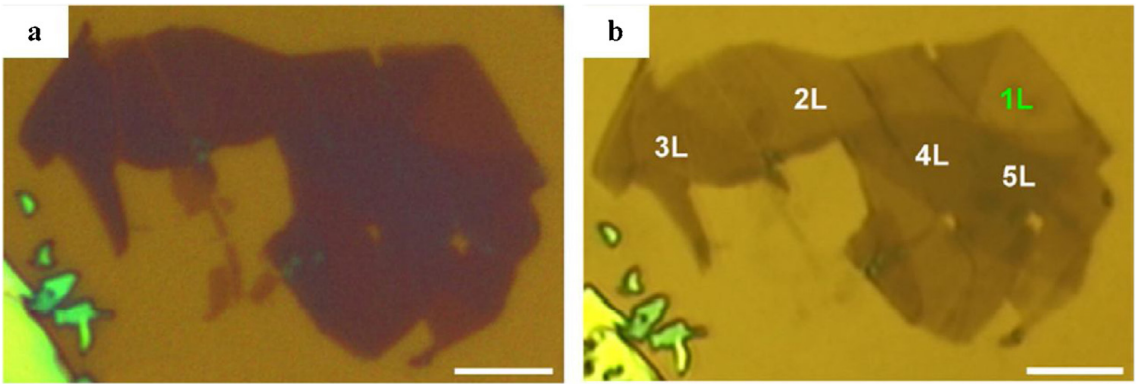

Fig. I.3. coupled mechanical exfoliation and subsequent thinning of the Ar+ plasma. (A) An optical picture of mechanically exfoliated multilayered pure phosphorene. (b) After Ar + plasma thinning of (A): (scale bar: 500 nm) [8, 9].

In the preparing operation, BP bulk was exfoliated using bath sonication for 24 h in N-methyl-2-pyrrolidone (NMP), followed by high-speed centrifugation to get the steady scuttles of phosphorene. This work was pursued by a wave of studies on the preparation of phosphorene via LPE with various experimental parameters. Based on thermodynamic theories, the liquid phase exfoliation should be better with lower variation of surface energies between 2D materials and solvents [3]. Organic solvents are the most famous and common media for liquid exfoliation. For the production of phosphorene, Different types of organic solvents have been used.

In order to get the best solvent for liquid exfoliation, Kang et al. exfoliated BP in acetone, chloroform, hexane, ethanol, IPA, DMF and NMP. They proved that the concentration of BP scuttles increased with boiling point and surface tension of solvents (Fig.I.4) and NMP was the optimal solvent for producing steady BP suspensions with the highest concentration [3].

In Different study, Woomer et al [4]. inspected 18 solvents and found that benzonitrile was the best for its ability to yield the highest BP suspensions concentration. To some extent, the diverse.

In order to understand the interaction between solvents and BP at the microscopic

scale, Sresht et al [3, 4]. modeled the LPE of BP through molecular dynamics (MD) simulations. It was concluded that an overall design of LPE experiments was based not only on the energetics but also on the organizing and the geometry of solvent molecules at the phosphorene-solvent interface.

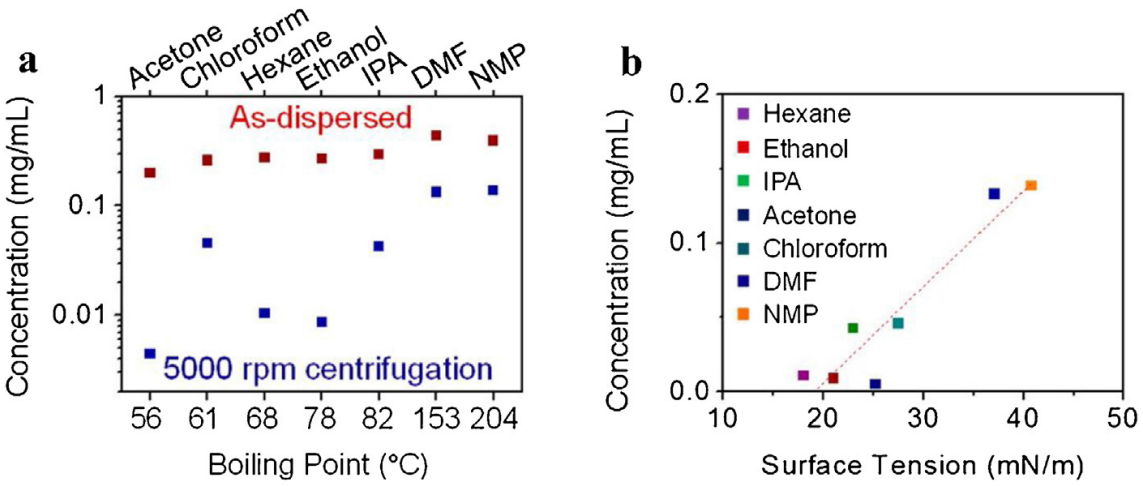

Fig. I.4. Exfoliation in liquid phase using various organic solvents. (A) The concentration of BP for several solvents with varied boiling points after and before 5000 rpm centrifugation. (b) After 5000 rpm centrifugation, BP plot of concentration for various solvents with varied surface tensions [8, 4].

I.5.black Phosphorus Properties

I.5.1. Structural Properties

The orthorhombic crystalline structure of BP is made up of parallel double layers that are wrinkled [12]. Each double layer's two halves are made up of a parallel zigzag chain of phosphorus atoms that are linked together. The structure's five phosphorus atoms each have five valence electrons in their 3p orbitals, which are filled by forming covalent bonds and give rise to sp3 hybridization. The top and bottom halves of the double layer are held together by three covalent bonds, two of which are in

the same plane and one of which is connected to an atom of phosphorus above or below [12]. The quadrangular pyramid shape of P6 rings in the chair form results from each phosphorus atom having a single electron pair left over as a result (Fig. I. 5). The zig-zag chain's direct link between two phosphorus atoms is 2.224 Å, which is roughly equal to the distance between the two chains in the upper and lower parts of the double layer (2.244 Å). With an average angle of 102º, the lowest P-P distance between two double layers is 3.314 Å [12]. Lattice constants and angles may vary with the number of layers, according to recent studies. The bulk BP multilayer or the phosphorene few layer structure is created by weak van der Waals forces stacking individual wrinkled layers together. [12]

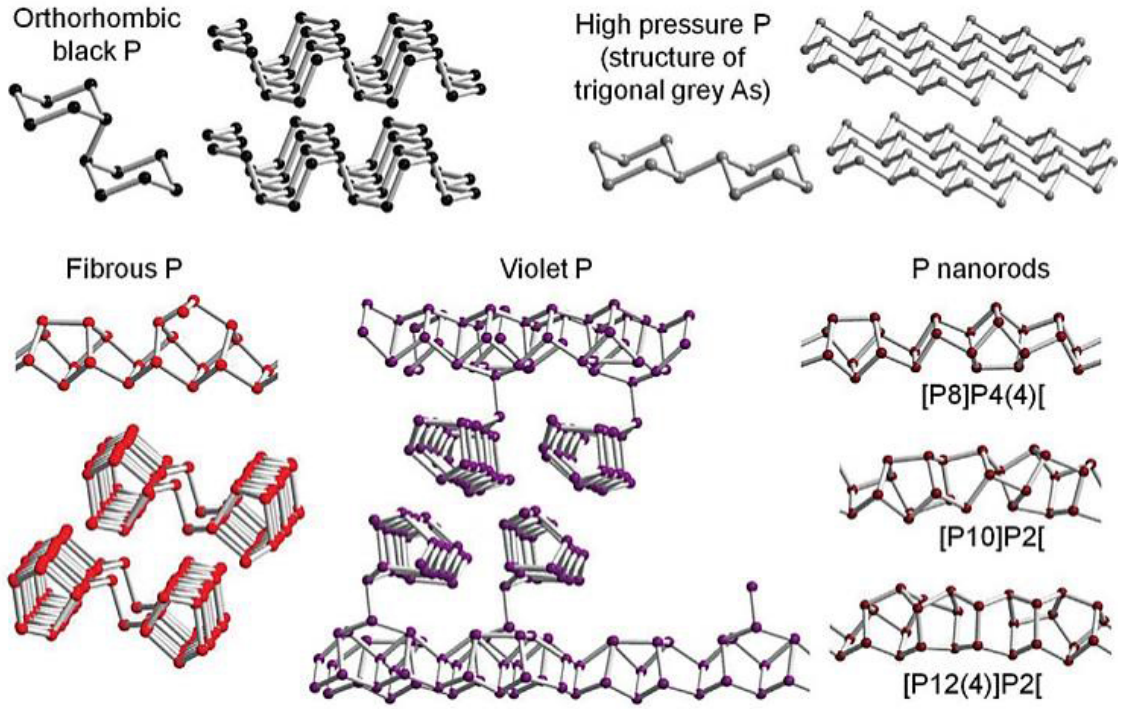

Fig. I.5. Fragments of multilayer and tubular allotropes of phosphorus with distinctive structural properties [12].

I.5.2. Chemical properties

The amount of ambient BP stabilization is relatively little. Long-term exposure to ambient conditions causes BP to degrade, with its surface oxidizing to form PxOy and then reacting to form phosphoric acid [12]. In a typical laboratory environment, within a few hours, the breakdown of a few layer BP can be seen. Martel et al. recently

clarified the mechanism, demonstrating that this degradation is thickness dependent and progresses with fewer layers due to the quantum confinement effect. If exposed to ambient light and air, BP becomes uniformly covered in tiny droplets of phosphoric acid measuring ~100 μm in size [12]. The basal plane of these nucleation sites grows more than the edge. These droplets eventually agglomerate after several days. It's interesting to see that the degradation declines significantly in the absence of light. It was demonstrated that the deterioration is photo-induced and occurs when oxygen and water vapor are present while being exposed to light [12]. There have also been reports of thermal degradation of exfoliated BP occurring continuously at ~400°C in vacuum until only a thin, amorphous red P like skeleton is left [12].

The oxidation is layered; BP is consequently thickness dependent [12], due to the fact that fewer layers cause the band gap to move to higher energies and cause the BP band edge and oxygen acceptors to overlap more strongly. According to oxygen concentration and light intensity, the rate of BP oxidation rises lin early [12].

Nevertheless, the investigation's first 2D substance to noticeably degrade when exposed to ambient air is BP. The main issue, which previously was the deterioration brought on by air and water in the BP case, has now been replaced by worries about metallic and oxidation debris during the production of carbon nanomaterials [12]. There was a propensity to refer to multilayer BP as "stable" or "passivated" BP when addressing its production and use as soon as its stability was questioned [12, 6].

I.5.3. Physical properties

BP is semiconductive and exhibits strong intrinsic in-plane anisotropic physical properties, including layer-dependent photoluminescence and a direct bandgap(0.3 to 2.3 eV) , as a result of its distinctive puckered structure and van der Waals, with a relatively limited carrier mobility ambient temperature (~1000 $cm^2 V^{-1} s^{-1}$), It has found applications in FET batteries. Innovative (opto)electronic devices should have anisotropic properties, and this material's significant in-plane anisotropy can help make these devices possible [12].

BP belongs to the group of substances called topological insulators [12]. As a result, both diamagnetic and paramagnetic behavior can be seen depending on the direction in the magnetic field, making the magnetic characteristics highly anisotropic.

[12].Compared to other 2D layered materials, BP has a direction-dependent Young's modulus 2, which is one order of magnitude smaller.
According to theoretical research, monolayer BP in-plane stresses could significantly change its electronic band structure, the carrier's mobility changes dramatically and anisotropically in zigzag and armchair directions [12]. Recently, it was demonstrated that monolayer BP is auxetic3 when a uniaxial force is applied in a zigzag direction [12]. According to recent reports, Young's modulus of few-layer BP is ~58 and ~27 GPa in armchair and zigzag directions respectively, with extremely anisotropic transport behaviour in BP and derived the conductance anisotropy of 63.7% [12, 7].

Overall, BP's unique big magnitude in-plane anisotropic 4 physical properties are what set it apart from other 2D layered materials (electrical, magnetic, thermal, vibrational, mechanical and spectroscopic). Recent reviews of the BP anisotropic characteristics have been conducted, and in-depth discussions of the topic can be read elsewhere [12, 8].

I.6. Phosphorene Applications

I.6.1. Batteries :

One of the most popular power sources for a wide range of portable electronic gadgets is lithium-ion batteries (LIB). Currently, commercial materials with low theoretical capacities, including graphite, are employed as anodes for commercial LIB [12, 9].

As trustworthy alternatives, new materials with greater capacity are being energetically sought after. Because of their excellent gravimetric, low polarization, and volumetric capabilities, transition metal phosphides were one of them and were thought to make viable anode materials. However, due to the usage of heavy transition metals, the anodes' energy densities were poor. For LIB, using BP directly as an anode material is being studied as an alternative to increase energy density [12].

Theoretical specific capacity of BP as a material for negative electrodes, with the majority of its capacity at the discharge potential range.

The BP particles electrodes' hexagonal copper phosphide (Cu_3P), which the scientists assigned the reversible LIB capacity to, was identified through structural investigations. Recent theoretical research based on calculations utilizing the density

functional theory (DFT) confirms that BP is anticipated to offer numerous applications in high-performance LIB [12, 10], Na-ion batteries (SIB). and Mg-ion batteries (MIB).

I.6.2. Field Effect Transistors

The distinctive anisotropy of charge transport results in significant performance enhancements in BP as compared to other 2D semiconductors. It was reported that the first p-type FET used a few layers of BP and SiO_2 as the gate insulator by Li et al. the drain current modulation dropped monotonically as sample thickness grew, while The mobility peaks at ~10 nm and decreases somewhat above this. At ambient temperature, the BP FET displayed ambipolar behavior with drain current modulation up to ~105 and field effect mobility up to 984 $cm^2 V^{-1} s^{-1}$ [12].

metallic elements are injected into BP layers using electron doping. also demonstrated to be a viable route to high performance and more reliable BP FET. Cu adatoms function as an electron donor and n-dope the BP layers, according to first principles investigations, without impairing the layers' structural integrity [12, 11].

I.6.3. Applications of phosphorene for sensing

I.6.3.1 Gas sensing

Due to their extremely high surface activities and enormous surface-to-volume ratios, 2D nanomaterials have recently demonstrated a great deal of promise as candidates for room-temperature sensing layers [12, 12]. BP may be used to detect various gas molecules and is sensitive to the atmosphere around it.

By first principle calculations, Kou et al. first assumed that BP would perform better as a gas sensor than its 2D competitors. They examined the monolayer BP's structural, electrical, and transport characteristics when CO, CO_2, NH_3, NO, and NO_2 were adsorbed on it. It was discovered that phosphorene was more vulnerable to gas molecules made of nitrogen, such as NO and NO_2 [12]. They explained the phenomenon by the charge transfer and alteration of the electronic band structure brought on by the adsorption of gas molecules. According to transport simulations, NH_3 absorption decreased the current while NO absorption had the opposite effect. Inspired by the theoretical study, Abbas et al produced the first BP gas sensor [12]. In their study, a FET-based sensor (Fig.I.6a) was made with BP flakes that were exfoliated

mechanically. The degradation caused by exposure to gas molecules was decreased by using comparatively thick BP flake while taking the sensor stability into account.

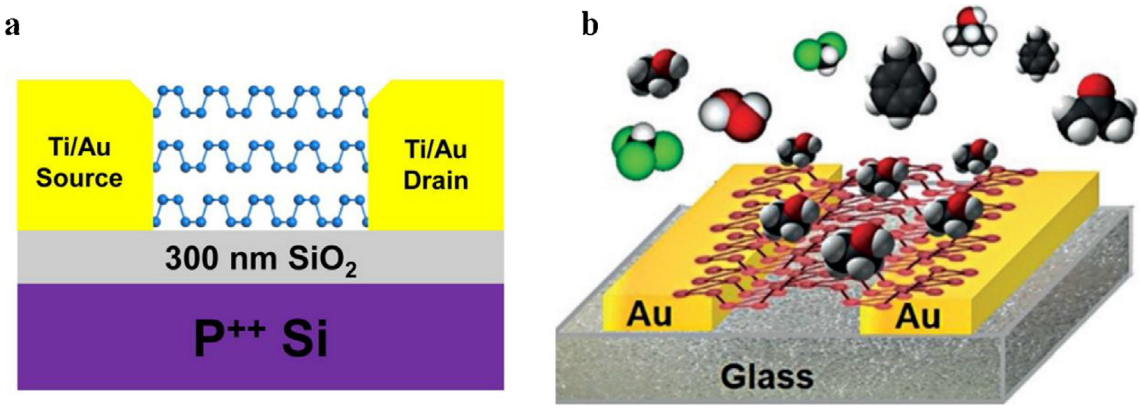

Fig. I.6 gas-sensing devices configurations's. (a) (FET) [12, 13], (b) Chemiresistor [12,14].

I.6.3.2 Humidity sensing

Graphene, MoS2, h-BN, and other 2D materials are less unstable than BP in the presence of water and air [12, 15]. Applications for BP are hampered by its low ambient stability under atmospheric conditions. It's intriguing, though, that some researchers used BP's hydrophilicity to create humidity sensors.

Yasaei et al. BP flakes were used to construct the first BP humidity sensor. The LPE method was used to create the BP films for the investigation. Gallium-Indium Eutectic was used to cut the prepared BP films into the necessary forms with two electrical contacts [12].

Yao et al [16]. revealed a novel humidity sensor made of stacked BP nanosheets in a quartz crystal microbalance (QCM). According to Sauerbrey's connection, QCM is a mass sensing platform that can identify changes in mass at the subnanogram level [12, 16]. A QCM may convert the adsorbed molecular mass to a frequency-dependent signal based on the connection. To created the QCM humidity sensors, Yao et al. deposited BP nanosheets made using the LPE process on the electrodes of the QCMs. By adjusting the relative humidity level and seeing how the resonance frequency changed, the humidity sensing properties were quantified [12]. It was discovered that as humidity increased, the resonance frequency decreased. The recovery and response times were quick to be 14 s and 10 s, respectively. At a high humidity level of 97.3%, the resonance

frequencies of QCM humidity sensors were measured every 4 days for 4 weeks and showed sustained stability [12].

I.6.3.3 Photodetection

Obtaining high responsivity together with ultrafast response encompassing wide spans of electromagnetic spectrum detection is the primary problem for photodetectors based on 2D nanomaterials [12].

While TMDs are constrained by their slow reaction times and huge bandgaps, graphene suffers from weak responsivity and the absence of a natural bandgap [12]. Graphene is a strong choice to increase the detection range with high responsiveness due to the tunable direct bandgaps between it and the TMDs of BP. Additionally, its distinct in-plane anisotropic characteristics can be applied to photodetectors.

Bolometric effect, photovoltaic, photo-thermoelectric, and photoconductive are some of the ways by which photocurrent is generated. In our knowledge, Buscema et al. first looked into how well photodetectors based on FETs built of ultrathin (3–8 nm thick) BP performed in the visible range up to 940 nm. The BP transistors had a response up to 4.8 mA/W with a rise time of approximately 1 ms; upon 640 nm laser illumination. With a f3dB of 6.2 kHz, the rising time demonstrated quick and broadband detection. Additionally, they noted that as excitation increased, the responsiveness and f_{3dB} decreased, which they attributed, respectively, to a decrease in the number of photogenerated carriers available for extraction and an increase in the rate of recombination processes between photogenerated charge carriers. Regarding the detection range, BP also demonstrated a substantial reaction to ultraviolet (UV), mid-infrared (MIR) and terahertz (THz) spectral regimes [12].

Xiang et al [17]. reported efficient in situ surface functionalization using Cs_2CO_3 and MoO_3 overlayers for electron and hole doping on few-layer BP FET devices [12]. Upon the illumination of a 405 nm laser source, the responsivity of Cs_2CO_3 variation enhanced the responsivity from 0.58 to 1.88 AW^{-1}, whereas MoO_3-decorated BP photodetector boosted from 0.6 to 2.56 AW^{-1}. The Cs_2CO_3 and MoO_3 decoration enhanced the corresponding EQE from 178% to 576% and from 183% to 784%, respectively. Xiang et al. built a FET photodetector using BP that has been se-doped. With the illumination of a 635 nm laser source, the responsivity of the main BP photodetector was 0.765 AW^{-1} [12]. For the Se-doped photodetector, the responsivity was dramatically improved to be 0.765 AW^{-1}. Furthermore, the EQE of the

photodetector was enhanced from 149% to 2993%. Liu et al. stated that the electrical tuning of the BP bandgap was made possible by the large Stark effect in a few-layer BP device. The discovery of a large Stark effect controlled by an electrical gate in BP lays the possibility for the development of photodetector systems that can function across a broad electromagnetic spectrum [12]. Few layer BP films have a significant flaw in that they degrade quickly in ambient air. Na et al [18]. demonstrated a well applied Al_2O_3 passivation to produce an air-stable BP photodetector. During six months of operation in ambient air and even after chemical treatment, the BP photodetector displayed respectable near-infrared performance with no evidence of degradation [12].

I.6.3.4 Biosensing

BP has proven to be suitable for biosensing applications [12, 19]. According to reports, BP possesses a significant amount of innate electrochemical activity, and is employable in biosensing schemes. A few-layer BP-based non-enzymatic hydrogen peroxide (H_2O_2) electrochemical sensor was reported [12, 19]. The BP electrode was made by casting BP nanosheet solutions over a glass carbon electrode that had already been treated. The detection limit of the H_2O_2 sensor was exceptional, measuring 1×10^{-7}.

Mayorga-Martinez et al. found that compared to black phosphorus macroparticles, it was discovered that BP nano-particles (NPs) had an improved catalytic effect on the hydrogen evolution reaction (HER). So, in a competitive immunoassay for rabbit immunoglobulin G (IgG) detection using HER, they chose to use BP NPs as electrocatalytic tags. The detection system's low detection limit for rabbit IgG was 0.98 ng/mL, with a linear range from 2 to 100 ng/mL [12, 19].

In addition to BP's inherent electrochemical activity, BP NPs' fluorescence can be used for biosensing. BP NPs were used as a novel nanomaterial in fluorescence-based nucleic acid detection, it was reported by Yew et al. The affinities of tagged single-stranded (ss-DNA) and double-stranded (ds-DNA) DNA oligonucleotides for spontaneous self-assembly with BP NPs were used as the basis for this detection approach.

The FET biosensor could identify human IgG with a reaction time of seconds and a low detection limit of 10 ng/ml. Additionally, it was discovered that the sensor showed a high selectivity for human IgG. Due to its ease of use, practicality, low cost, and quick/direct reading with the naked eye, colorimetric detection for biomolecules has

received a lot of interest [12, 19]. In order to increase catalytic activity and create colorimetric biosensors for detecting carcinoembryonic antigen (CEA), the instability or stability-related restriction of BP was employed [19]. In the work, 4-nitrophenol (4-NP) reduction was successfully catalyzed by Au Nps adorned few-layer BP.

I.6.3.5 Ion sensing

Detecting trace heavy metal ions is crucial since they may cause human cancer. Examples of these ions are Hg2+, Pb2+, Cd2+, and AsO2. Energy dispersive X-ray fluorescence (EDXRF) is one of the most accurate techniques for identifying heavy metal ions [12, 20], The difficulties of laboratory-based techniques can be overcome by atomic chemical sensors based on BP FETs, enabling quick label-free detection with a straightforward procedure and low cost. An air-stable ion sensor based on BP FET encased with ionophore was disclosed by Li et al [20]. The ionophore film can both selectively permit specific types of molecules to pass through it and eliminate harmful elements from the surrounding environment. The BP sensors were able to recognize Pb^{2+}, Cd^{2+}, AsO^{2-} and Hg^{2+} down to 1, 3, 10, and 1 ppb, respectively, within the permitted range of the World Health Organization's (WHO) drinking water quality recommendation. They have recently revealed the development of another Hg^{2+} sensor based on BP FET [12, 20]. like the BP gas sensor created by Lee et al, The suspended few-layer BP channel served as the basis for the FET Hg^{2+} sensors. The suspended structure's heightened sensitivity and extraordinary detection limit are the result of its optimal gating effect, increased sensing area, and reduced low frequency noise. The BP sensor could detect Hg^{2+} down to 0.01 ppb with response rate of only 3 s.

I.7. Major challenges and future trend

Compared to graphene and TMDs, BP has garnered a lot of interest as a prospective option in a variety of sensing domains because of its puckered lattice structure, direct band gap, and distinctive electrical characteristics. However, the utilization of BP for wide-scale applications is now hampered by the difficulty of synthesizing it with the availability of large area flakes. Controlling the size and quantity of layers in BP samples while obtaining a high manufacturing yield of BP flakes is extremely difficult. If the layer number of BP can be carefully managed, its bandgap can be adjusted for a particular wavelength with the best response and dark current. Although BP production

using the mineralizer-assisted gas-phase transformation approach offers an effective option for the creation of big, high-quality crystals, there is still a great need for adaptable methods for high-throughput and scalable synthesis [12].

Another difficulty is that, like other 2D materials, defects in the production of phosphorene are unavoidable [12, 21]. There are numerous types of flaws in BP, including point defect, oxygen defect, grain boundary (GB) defect, and so forth. When compared to faults in other 2D materials, phosphorene defects have distinctive characteristics. In addition, phosphorene is more easily susceptible to faults than silicone and graphene, and its electrical characteristics are less responsive to defects [12, 21]. Due to the hanging connections they cause, flaws can enhance sensing performance, although further research is still needed.

The third difficulty is that the BP is easily damaged under ambient conditions, which is typically viewed as a bad quality and restricts the practical applications of BP. H_2O, O_2, and light were shown to have synergistic effects on the breakdown of BP by Zhou et al. in [21]. The majority of earlier experiments on BP sensing were conducted in unique, customized environments without a mixing of H_2O and O_2, therefore the BP sensor didn't show any evident signs of degradation [12]. According to Li et al. they demonstrated the first air-stable blood pressure sensor enclosed in an ionophore film that could both filter out undesirable elements from the surrounding environment and enable specific types of ions to pass through it. The protective layer with permselectivity is the best method for improving the air stability of the BP sensor without interfering with the interaction between the BP surface and the molecules being detected. However, it is quite difficult to locate a suitable film that has good permselectivity for the protective layer [12].

BP-based materials can be used in bio, ion, and gas sensing to identify minute quantities of a variety of analytes, such as gas molecules, hydrogen peroxide, DNA, immunomolecules, heavy metal ions, etc. through a number of methods: electrical, electrochemical, fluorescence, and colorimetric transduction, among other methods [12, 21].

I.8. Conclusion

In conclusion, this chapter presents an overview of the state-of-the-art research in black phosphorus and phosphorene including the crystal structure, chemical and physical properties, synthesis methods, advances and various applications... Some of the remarkable properties, advances and applications of black phosphorus and phosphorene, are highlighted in this chapter. Despite the significant properties and advances, research in this area is still in the very early stage compared to graphene and other well-explored 2D materials. This chapter also summarized recent progress in phosphorene and its future directions. The unusual structure of BP and phosphorene sets its aside from graphene and other widely studied 2D semiconductors.

References

[1] K. Tamersit, F. Djeffal, Double-Gate Graphene Nanoribbon Field-Effect Transistor for DNA and Gas Sensing Applications: Simulation Study and Sensitivity Analysis, IEEE Sensors Journal, vol.16, pp. 4180 – 4191, 2016.

[2] Cartz. L, Srinivasa. S. R, Riedner. R. J, Jorgensen. J. D, Worlton. T. G, "Effect of pressure on bonding in black phosphorus," The Journal of Chemical Physics, vol. 71, pp.1718, 1979.

[3] V. Sresht, A. A. H. Pádua, D. Blankschtein, "Liquid-Phase Exfoliation of Phosphorene: Design Rules from Molecular Dynamics Simulations," ACS Nano, vol.9, pp. 8255–8268, 2015.

[4] J. Kang, J.D. Wood, S.A. Wells, J.-H. Lee, X. Liu, K.-S. Chen, M.C. Hersam, "Solvent Exfoliation of Electronic-Grade, Two-Dimensional Black Phosphorus," ACS Nano; vol. 9, pp. 3596–3604, 2015.

[5] A. Favron, E. Gaufres, F. Fossard, A.L. Phaneuf-L'Heureux, N.Y.W. Tang, P.L. Levesque, A. Loiseau, R. Leonelli, S. Francoeur, R. Martel, "Photooxidation and quantum confinement effects in exfoliated black phosphorus," Nat. Mater, vol. 14, pp. 826–832, 2015.

[6] J. Sun, G. Zheng, H. W. Lee, N. Liu, H. Wang, H. Yao, W. Yang, Y. Cui, "Formation of stable phosphorus-carbon bond for enhanced performance in black phosphorus nanoparticle-graphite composite battery anodes," Nano Lett, vol. 14, pp. 4573–4580, 2014.

[7] J. Tao, W. Shen, S. Wu, L. Liu, Z. Feng, C. Wang, C. Hu, P. Yao, "Mechanical and Electrical Anisotropy of Few-Layer Black Phosphorus," ACS Nano, vol. 9, pp. 11362–11370, 2015.

[8] A. Carvalho, M. Wang, X. Zhu, A. S. Rodin, H. Su, A. H. Castro Neto, "Phosphorene: from theory to applications," Nat. Rev. Mater, vol. 1, pp. 1-16, 2016.

[9] R. Yazami, P. Touzain, "A reversible graphite-lithium negative electrode for electrochemical generators," J. Power Sources, vol. 9, pp. 365–371, 1983.

[10] K. Hembram, H. Jung, B. C. Yeo, S. J. Pai, H. J. Lee, K.-R. Lee, S. S. Han, "A comparative first-principles study of the lithiation, sodiation, and magnesiation of black phosphorus for Li-, Na-, and Mg-ion batteries," Phys. Chem. Chem. Phys, vol.18, pp.21391–21397, 2016.

[11] Y. Pan, Y. Wang, M. Ye, R. Quhe, H. Zhong, Z. Song, X. Peng, D. Yu, J. Yang, J. Shi, J. Lu, "Monolayer phosphorene–metal contacts," Chem. Mater, vol. 28, pp. 2100–2109, 2016.

[12] A.J. Yang, D.W. Wang, X.H. Wang, J.F. Chu, P.L. Lv, Y. Liu, M.Z. Rong, "Phosphorene: A Promising Candidate for Highly Sensitive and Selective SF6Decomposition Gas Sensors," IEEE Electron. Lett, vol. 38, pp. 963–966, 2017.

[13] A.N. Abbas, B. Liu, L. Chen, Y. Ma, S. Cong, N. Aroonyadet, M. Köpf, T. Nilges, C. Zhou, "Black phosphorus gas sensors," ACS Nano, vol. 9, pp. 5618-5624, 2015.

[14] C.C. Mayorga-Martinez, Z. Sofer, M. Pumera, "Layered Black Phosphorus as a Selective Vapor Sensor," Angew. Chem, vol. 54, pp. 14317–14320, 2015.

[15] J.S. Kim, Y. Liu, W. Zhu, S. Kim, D. Wu, T. Li, A. Dodabalapur, K. Lai, D. Akinwande, "Toward air-stable multilayer phosphorene thin-films and transistors," Sci. Rep, vol. 5, pp. 8989, 2015.

[16] Y. Yao, H. Zhang, J. Sun, W. Ma, L. Li, W. Li, J. Du, "Novel QCM humidity sensors using stacked black phosphorus nanosheets as sensing film," Sens. Actuators B, vol. 244, pp. 259–264, 2017.

[17] D. Xiang, C. Han, J. Wu, S. Zhong, Y. Liu, J. Lin, X.A. Zhang, H.W. Ping, Ö. B, A.H. Neto, "Surface transfer doping induced effective modulation on ambipolar characteristics of few-layer black phosphorus," Nat. Commun, vol. 6, pp. 6485, 2015.

[18] J. Na, K. Park, J.T. Kim, W.K. Choi, Y.W. Song, "A study of bilayer phosphorene stability under MoS2-passivation," Nanotechnology, vol. 28, pp. 085201, 2017.

[19] M. Pumera, " Phosphorene and black phosphorus for sensing and biosensing," TRAC Trends Anal. Chem, vol. 93, pp. 1–6, 2017.

[20] P. Li, D. Zhang, C. Jiang, X. Zong, Y. Cao, "Ultra-sensitive suspended atomically thin-layered black phosphorus mercury sensors," Biosens. Bioelectron, vol. 98, pp. 68–75, 2017.

[21] V. Wang, Y. Kawazoe, W.T. Geng, "Native point defects in few-layer phosphorene," Phys. Rev. B, vol. 91, pp. 045433, 2015.

Chapter II

Density functional theory

Abstract: Density functional theory (DFT) has developed over the past few decades from a rising star to one of the main actors in computational quantum chemistry. This theme issue aims to provide an overview of a few DFT-related topics.

II.1 Introduction

Density functional theory (DFT) is a quantum-mechanical (QM) method utilised in chemistry and physics to calculate the electronic structure of atoms, molecules and solids. It has been very popular in computational solid-state physics since the 1970s [1]. Its goal is the quantitative understanding of material properties from the fundamental laws of quantum mechanics. (DFT) is a low-cost, time-saving quantum mechanical (QM) theory, used to compute many physical characteristics of solids with high precision [2]. The foundations of density-functional theory are the Hohenberg–Kohn and Kohn–Sham theorems which can easily be extended from its original formulation to cover a wide variety of physical situations [3]. The history to DFT's success is the quest for the exchange-correlation functional, which utilizes density to represent advanced many-body phenomena inside one element formalism. If a precise exchange-correlation functional is applied, it may correctly describe the quantum nature of matter. The estimated character of the exchange-correlation functional is the basis for DFT implementation success or failure [2]. This chapter is aimed to present an overview of DFT by describing the theoretical foundations, widely used approximations, current advances, and issues addressed, as well as future horizons.

II.2 What is Density Functional Theory (DFT)?

Density functional theory (DFT) is a quantum-mechanical atomic simulation method to count a large diversity of properties of nearly any type of atomic system: molecules, crystals, surfaces, and even electronic devices when combined with non-equilibrium Green's functions (NEGF) [2].

DFT belongs to the family of first principles (ab initio) methods, so called because they can portend material properties for unbeknown systems without any experimental input. Within these, DFT has earned popularity because of the relatively low arithmetic effort required [2].

The DFT approach is largely utilised in organic and inorganic chemistry, materials sciences like metallurgy or ceramics, and for electronic materials, to just name a few areas [2].

II.3 A very brief historical background

The ground-breaking developments of quantum mechanics in the early 20th century lastly provided the answer to many superb questions about the nature and properties of the atom. Applying these principles to more complex systems such as molecules and solid-state materials demonstrated harder, but; even in classical physics there is no general solution to a three-body problem (such as the combined orbital movement of the sun, the moon, and the Earth), and to depict just a water molecule we have to transact with ten electrons and three atomic nuclei [2].

The success and applicability of DFT lies in some very bright recognition in the mid-1960s by Walter Kohn, Pierre Hohenberg, and Lu Jeu Sham. By not focusing on the individual electrons but instead using the electron density as the main variable to solve for, and moreover reformulating the many-body problem as an equal single-particle problem, density functional theory was born [2].

Through the next decades many contributors turned the method into a practical tool, and through the utilisation of powerful numerical computers, DFT became a necessary tool for materials science, chemistry, and many other fields. Relatively explicit plugins of the spin degree of freedom have enabled the description of magnetic systems, and on top of that, relativistic effects and even superconductivity can be processed [2].

II.4. What problems does DFT solve?

Atomic modeling in general, and DFT calculations particularly, supply considerable value to researchers and scientists working with chemicals, electronic materials, etc..., in two distinct parts: [2, 3]

- As it can treat basically any element in the periodic table in any kind of atomic arrangement, without the need for experimental input parameters, DFT has sturdy predictive strength, even for completely novel molecules or materials. In this way, atomic simulations can minimize evolution time and cost by down-picking of promising material candidates before to going into the lab and dealing with costly and perhaps dangerous chemicals with unknown properties and attitude. Via high-performance computer (HPC) clusters, one person can screen hundreds or even thousands of materials at the same time, immensely exceeding the number of simultaneous experiments that a human can carry out [2].

- Second, DFT calculations are used to better understand how materials and devices act and function under various conditions. A drilled DFT user can compare measurement data to simulation output to make educated guesses regarding the physical cause of some phenomena that are observed in the material or device but are difficult to depict using straightforward models. In order to fully utilize the effects and material in question, as well as to go even farther in order to, for instance, minimize device dimensions or improve material options or method terms, such vision is essential [2].

DFT is therefore an essential tool for technology pathfinding, to discover novel materials and strange physical phenomens, due to its predictive capabilities and atomic quantum-mechanical quality, before a top-tier attempt device is made, or also before a new material has undergone full experimental characterization [2]

II.5 Fundamentals of DFT

Density functional theory [3] can be used to numerically solve the Kohn-Sham equation, a single particle independent Schrodinger equation, which can be used to simplify the Schrodinger Equation [4] for a multiple body system. This computational procedure generates the solid's physical properties, although this hypothesis is based on electron density rather than wave functions, for which the scientist Walter Kohn won the 1998 Nobel Prize in Physics [3, 5]. Thomas and Fermi asserted total density is the key parameter in many body issues in 1927, despite the absence of exchange-correlation effects at the time [3, 6, 7]. The foundation for DFT was created in 1964 by the theorems of Hohenberg, Kohn, and Sham, which claimed that the functional of a many-body problem's (non-degenerated) ground state electron charge density could completely characterize all properties in the absence of a magnetic field [3, 8].

II.5.1 The Hohenberg - Kohn (HK) theorems

In 1964, Hohenberg and Kohn [3, 9] presented two seemingly straightforward theorems that allowed DFT to be used. They said in one of their theorems that the electron density that minimizes the functional field's overall energy corresponds to the genuine ground state density of an electron. Consider the situation where ρr represents the density of the system's ground state and ρ′(r) represents any other state of a many-body system. In this case, the functional for total energy is given as; Eρ′>Eρ. As well,

suppose that F[ρ(r)] is a general functional that is valid for fixed electrons at all external potentials. Mathematically This could be expressed as; [3]

$$F[\rho(r)]=T[\rho(r)]+U[\rho(r)] \quad \text{(II.1)}$$

Also,

$$E[\rho(r)]=\int[v(r)\rho(r)]dr+F[\rho(r)] \quad \text{(II.2)}$$

The associated density ρ(r) must essentially be a ground state density for it to be lowest energy functional [3].

$$E[\psi']=(\psi',V\psi')+(\psi',T+U)\psi' \quad \text{(II.3)}$$

Supposing ψ is ground state function corresponding to ρ(r) for external potential v (r), higher energy will be corresponding to ρ′(r), according to the variational principle.

$$E[\psi']=\int[v(r)\rho'(r)]dr+F[\rho'(r)]>E[\psi]= [v(r)\rho(r)]dr + F[\rho(r)] \quad \text{(II.4)}$$

Therefore, one may simply calculate the ground state density as well as energy in an established external potential supplied the density functional is adequately defined [3]. Additionally, it shows that ρ(r) reduce the energy functional E[ρ(r)].

II.5.2 The Kohn-Sham (KH) equations

Hohenberg-Kohn's theorems are precise but not very useful for actual calculations [10]. The Kohn-Sham equation [11] transformed DFT into a practical tool. They transformed the challenging problem of electrons interacting collectively in an external effective potential (V_{ext}) into electrons that are not interacting in V_{ext} and the total energy for an interacting electron ground state in a fixed potential, v(r) is; [3]

$$E[\rho(r)]=V[\rho]+U[\rho]+G[\rho] \quad \text{(II.5)}$$

Where comprehensive density functional G[ρ] grasps exchange-correlation, and is written as;

$$G[\rho(r)]=T_s\rho+E_{xc}\rho \quad \text{(II.6)}$$

$$E[\rho(r)]=Ts[\rho]+V[\rho]+U[\rho]+E_{xc}[\rho] \quad \text{(II.7)}$$

Ts[ρ] stands for the kinetic energy in a many-body system with non-interacting electrons, while V[ρ] represents the external potential created by the core's positive charge, U[ρ] represents the coulomb potential, and $E_{xc}[\rho]$ stands for the energy produced by exchange-correlation effects [3].

$$T_s[\rho(r)]=-\hbar^2/2m\sum_i^N\int\varphi_i*(r)\nabla^2\varphi_i(r)d^3r=T[\varphi i\sum(\rho)] \quad \text{(II.8)}$$

And

$$U[\rho]=[q^2/2\int\rho(r)\rho(r')/r-r']drdr' \quad \text{(II.9)}$$

$$V[\rho]=\int v(r)\rho(r)dr \quad \text{(II.10)}$$

The exchange correlation energy $E_{xc}[\rho]$ for a many-body system created by ρ(r) is presented by;

$$E_{xc}[\rho]=\int[\rho(r)\varepsilon_{xc}\rho(r)]dr \quad \text{(II.11)}$$

And

$$E_{xc}[\rho]=E_x[\rho]_{exchange}+E_c[\rho]_{correlation} \quad \text{(II.12)}$$

The E_x term refers to the energy loss caused by antisymmetrization and can be shown as a single particle orbital as;

$$E_x=\int[\rho(r)\varepsilon_x\rho(r)]dr \quad \text{(II.13)}$$

And

$$E_c=\int[\rho(r)\varepsilon_c\rho(r)]dr \quad \text{(II.14)}$$

And

$$\varepsilon_x[\varphi_i\rho(r)]=-q^2/r\sum_{j,k}\int d^3r'(r)\varphi_k*(r)[\varphi_j*(r')\varphi_k*(r')\varphi_k(r)/r-r'] \quad \text{(II.15)}$$

Whereas the sole term in the summation is the energy of a molecule 'j' at site 'r' in comparison to a molecule 'k' at 'r''. The interacting particles, such as electrons that are anti-parallel and lower their energy by equally distributing their moments, mutually avoid one another, further reducing the energy of the system. KohnSham mapping of interacting and non-interacting system is presented in **Figure II. 1** [3].

$$\varepsilon_c=\sum_{j<k}q^2/r-r'=q^2/2\int d^3r\int[\rho(r)\rho(r')-\rho(r)\delta(r-r')/r-r']d^3r' \quad \text{(II.16)}$$

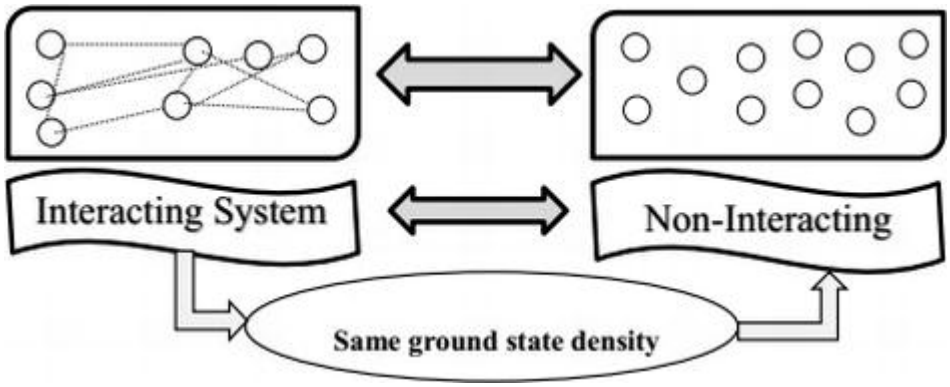

Figure II.1. Kohn-Sham mapping of non-interacting and interacting system. [3]

The energy of ground state may be acquired by differentiating Eq. (III.5) with respect to ρ(r)

$$0=\delta E[\rho]/\delta\rho(r)=\delta T_s[\rho]/\delta\rho(r)+\delta U[\rho]/\delta\rho(r)+\delta V[\rho]/\delta\rho(r)+\delta E_{xc}[\rho]/\delta\rho(r)=\delta Ts[\rho]/\delta\rho(r)+ v(r)+V_c(r)+E_{xc}(r) \quad \text{(II.17)}$$

By utilising density $\rho_s(r)$, the lower state for a non-interacting many-body system is;

$$0=\delta E_s[\rho]/\delta\rho_s(r)=\delta T_s[\rho]/\delta\rho s(r)+\delta V_s[\rho]/\delta\rho_s(r)+\delta V_s[\rho]/\delta\rho_s(r)=\delta Ts[\rho]/\delta\rho_s(r)+v_s(r) \quad \text{(II.18)}$$

Equating Eqs. (II.17) and (II.18), the potential V_s can be acquired as;

$$v_s=V(r)+V_c(r)+V_{xc}(r) \quad \text{(II.19)}$$

The equation for a one-particle system that is non-interacting in potential $v_s(r)$ can be derived from the equation of interacting electrons of the system in the subsistence of v(r) [3].

$$[(-\hbar^2/2m)\nabla 2+v_s(r)]\varphi_k(r)=E_k\varphi_k(r) \quad \text{(II.20)}$$

The ρ(r) of an authentic system is reproduced by orbitals, where f_k is the kth orbital occupation, and can be written as; [3]

$$\rho(r)=\rho_s(r)=\sum_k^N f[\varphi_k(r)]^2 \quad \text{(II.21)}$$

II.5.3 Exchange-correlation potential

The KS scheme's results showed that the energy functional's limiting energy may be used to determine the least energy state, and this can be done by finding an agreeable solution to a set of single-particle equations. In the KS scheme, There is only one major issue is that E_{xc} (exchange-correlation energy) cannot be precisely found. If E_{xc} is precisely determined, it is a accurate solution for a many-body problem. There isn't an exact solution available right now, therefore approximations are utilised to valuate E_{xc} with LDA and GGA being the most usually used approximations [3].

II.6 Commonly used exchange-correlation approximations

The exchange contribution was first described by Bloch (1929), and it has gained popularity cause of quantum Monte-Carlo simulations of uniform gases [3, 12]. The Local Density Approximation (LDA) [3, 13], suggested by Kohn and Sham, confirms that the exchange-correlation functional in any location in the space merely depends on that location's spin density. The Generalized Gradient Approximation (GGA) [3, 14, 15] is an expansion to the LDA component that contains terms that rely on density derivatives. Perdew was the first to submit an application of real-space cutoffs to produce GGAs, which resulted in the creation of the PW86 functional model [3, 14]. The PW91 functional [3, 16] was the zenith of this extensive development, and It generates beneficial accuracy for binding energies, as demonstrated in 1993 of around

6–10 kcal/mol [3, 17]. PBE [3, 18] is the most requently employed GGA to examine materials today. A hybrid GGA [3, 19] is one that joins an ordinary GGA plus a HartreeFock component, in which the kinetic energy density is additionally used to determine the 6 Density Functional Theory - new perspectives, recent advances and applications GGA component. The Density Functional (DF) includes a portion of GGA, LDA, Hartree-Fock exchange or hybrids, and/or a meta-GGA, frequently known as the exchange-andcorrelation (XC) functional (meta-GGA or meta-hybrid) [3]. A comparison of simplicity versus accuracy of existing approximations in DFT is shown in Figure II. 2. The functionals actually used in DFT simulations shape a natural hierarchy, and no systematic process to the accurate functional can be asserted [3]. The functional form that is now accessible is obviously improving, leading to a significantly more precise exemplification of ground state features. The most significant recent developments are those that in some way take into account the non-local part of the exchange potential. Table II.1, summarizes the present hierarchy [3].

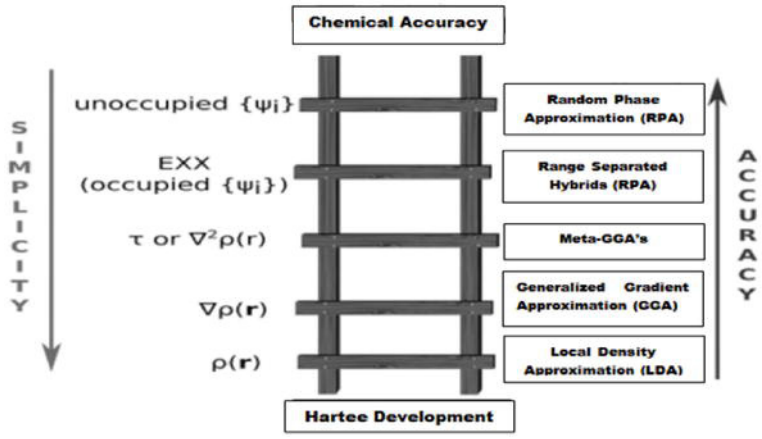

Figure II.2. A comparison of accuracy of current approximations vesus simplicity in DFT [3 , 20].

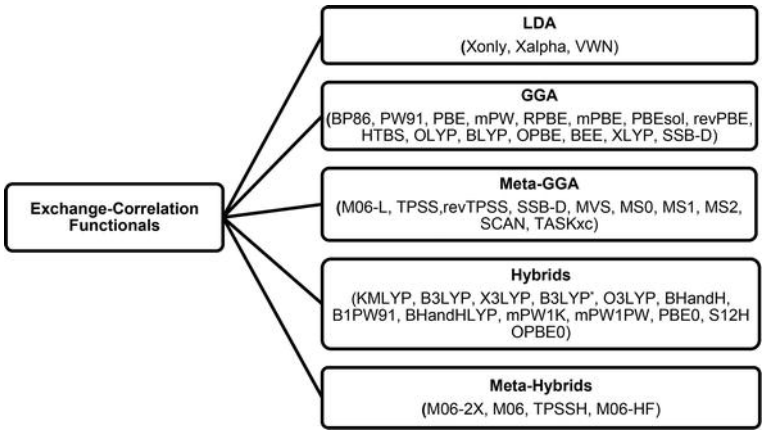

Table II.1. Commonly used Exchange functionals [3].

II.7 Weak interactions(Recent developments)

Strong progress has been achieved in solving the problems brought on by weak van der Waals (vdW) interactions over the past two decades [3]. Traditional functionals are effective manipulators of covalent, ionic, and metallic interactions cause of their semi-local nature, however, they fall short in terms of weaker, longer bonds, and cannot present weak binding that falls off as a function of R6 (R is the separation between two atoms) [3, 21]. The conventional functionals must be modified in order to take these effects into account, and there are three approaches to do this [3]. A series of approximations have been made by Langreth, Lundqvist, and collaborators [3, 22] While these approximations are produced non-empirically, they particularly start with contributions of correlation energy for the growth of explicit non-local functionals of electron density. These functionals have been created by assuming systems that contain a gap and may be beneficial for any materials, ranging from solids to molecules [3, 23].

II.8. Computational details

To investigate the developments of crystal structures, electronic structures, and physical properties, we first attain the stable crystal structures of black phosphorus within the framework of density functional theory (DFT) utilising the projector augmented wave (PAW) method [24]. These structures are optimized by employing the DFT-D3 method, so as to take into consideration the interlayer van der Waals force in bulk black phosphorus [25, 26].

II.9. Conclusion

Density Functional Theory is a commonly and powerful used quantum mechanical tool for investigating several aspects of matter. Such computations' accuracy is dependent on the creation of approximations for the exchange-correlation energy functional. There are ongoing efforts to design and improve density functionals because there are still problems to be overcome, it is a quantum fantasy to get all of the qualities right at a reasonable computing cost. High-parameterized functions that are adapted to the characteristics of molecular systems typically perform slightly better than functions that are lightly parameterized for molecules, but they typically perform rather badly in simulations on periodic materials.

References

[1] Tanja. van Mourik, Michael. Bühl, Marie-Pierre. Gaigeot, "Density functional theory across chemistry, physics and biology," Philos Trans A Math Phys Eng Sci, vol. 372, pp. 20120488, 2014.

[2] "Density Functional Theory," www.synopsys.com, https://www.synopsys.com/glossary/what-is-density-functional-theory.html.

[3] Muhammad. Aamir. Iqbal, Naila. Ashraf, Wajeehah. Shahid, Deeba. Afzal, Faryal. Idrees, Raice. Ahmad, "Fundamentals of Density Functional Theory: Recent Developments, Challenges and Future Horizons," 2021.

[4] Tsutsumi. Y, "Schrodinger equation," Funkcialaj Ekvacioj, vol. 30, pp. 115-125, 1987.

[5] Kohn. W, Sham. L.J, "Selfconsistent equations including exchange and correlation effects," Physical review, vol. 140, pp. A1133, 1965.

[6] Thomas. L. H, "The calculation of atomic fields," Mathematical proceedings of the Cambridge philosophical society, pp. 542-548, 1927.

[7] Fermi. E, "Statistical method to determine some properties of atoms," Rend. Accad. Naz. Lincei, vol. 6, pp. 5, 1927.

[8] Lundqvist. S, March. N.H, "Theory of the inhomogeneous electron gas," 2013.

[9] Gilbert. T. L, Hohenberg-Kohn, "Theorem for nonlocal external potentials," Physical Review B, vol. 12, pp. 2111, 1975.

[10] Gilbert T. L, Hohenberg-Kohn, "theorem for nonlocal external potentials," Physical Review B, vol. 12, pp. 2111, 1975.

[11] Kohn. W, Sham. L. J, "Selfconsistent equations including exchange and correlation effects," Physical review, vol. 140, pp. A1133, 1965.

[12] Ceperley. D. M, Alder. B. J, "Ground state of the electron gas by a stochastic method," Physical review letters, vol. 45, pp. 566, 1980.

[13] Gross. E. K, Kohn. W, "Local density-functional theory offrequency-dependent linear response," Physical review letters, vol. 55, pp. 2850, 1985.

[14] Perdew. J. P, Yue. W, "Accurate and simple density functional for the electronic exchange energy: Generalized gradient approximation," Physical review B, vol. 33, pp. 8800, 1986.

[15] Perdew. J. P, Wang. Y, "Accurate and simple analytic representation of the electron-gas correlation energy," Physical review B, vol. 45, pp. 13244, 1992.

[16] Burke. K, Perdew. J. P, Wang. Y, "Derivation of a generalized gradient approximation: The PW91 density functional," Electronic density functional theory, pp. 81-111, 1998.

[17] Gill. P. M, Johnson. B. G, Pople. J. A, Frisch. M. J, al, "An investigation of the performance of a hybrid of HartreeFock and density functional theory," International Journal of Quantum Chemistry, vol. 44, pp. 319-331, 1992.

[18] Perdew. J. P, Burke. K, Ernzerhof. M, "Generalized gradient approximation made simple," Physical review letters, vol. 77, pp. 3865, 1996.

[19] Sousa. S. F, Fernandes. P. A, Ramos M. J, "General performance of 13 Fundamentals of Density Functional Theory: Recent Developments, Challenges and Future…," The Journal of Physical Chemistry A, vol. 111, pp. 10439-10452, 2007.

[20] Datta. S, Jana. D, "Semiconductor Physics: A Density Functional Journey," Cond-Mat.Mtrl-Sci, pp. 13050, 2010.

[21] Yip. S, Andreoni W, "Handbook of Materials Modeling: Methods: Theory and Modeling," editor. Springer, 2018.

[22] Dion. M, Rydberg. H, Schröder. E, Langreth. D. C, Lundqvist. B. I, al, "Van der Waals density functional for general geometries," Physical review letters, vol. 92, pp. 246401, 2004.

[23] Berland. K, Cooper. V. R, Lee. K, Schröder. E, Thonhauser. T, Hyldgaard. P, Lundqvist. B. I, al, "van der Waals forces in density functional theory: a review of the vdW-DF method," Reports on Progress in Physics, vol. 78, pp. 066501, 2015.

[24] Peng-Lai. Gong, Da-Yong. Liu, Kai-Shuai. Yang, Zi-Ji. Xiang, Xian-Hui. Chen,Zhi. Zeng, Shun-Qing. Shen, Liang-Jian. Zou, Hydrostatic pressure induced three-dimensional Dirac semimetal in black phosphorus, physical review. B. 93. 195434, 2016.

[25] Kebabi. A, Bentabet. A, Djeffal. F, Ferhati. H, Benmekideche. N, Benmakhlouf. A, & Chala. A, DFT study of X-doped (X= Cu, Ag, Au) boron nitride nanotubes for spintronic and optoelectronic applications, Optik, 225, 165863, 2021.

[26] H. Ferhati, F. Djeffal, F. AbdelMalek, "Towards improved efficiency of SnS solar cells using back grooves and strained-SnO2 buffer layer: FDTD and DFT calculations," Journal of Physics and Chemistry of Solids, Vol. 178, pp. 111353, 2023.

Chapter III

A novel broadband mid infrared phototransistor using BP capping layer

Abstract: ***We present a new broadband mid-Infrared (mid-IR) InGaZnO (IGZO) thin-film phototransistor (TF PT) based on both Black Phosphorus (BP) capping layer incorporating gold (Au) intermediate ultrathin-film. It is found that the proposed device shows high photodetection performances with a high current ratio exceeding 180 dB over a wide voltage window. Besides, it is revealed that the introduced ultrathin Au layer within BP enhances the absorbance capability over the mid-IR spectrum, which significantly improves the performance of the broadband mid-IR sensor.***

III.1 Introduction

Nowadays, phototransistors (PTs) are becoming the key technology in various emerging optoelectronic systems including environmental monitoring, Optical Wireless Communication Systems (OWCS), chemical detection and analysis, spectroscopy applications, flame detection and imaging [1, 2, 3, 4, 5]. This is mainly due to their ability to simultaneously providing optical-to-electrical signal conversion and amplification [3, 4, 5, 6]. Rapid progress has been made in developing PT devices using different silicon and organic platforms to achieve high photoresponsivity values over different spectral ranges [2, 3, 4, 5, 6]. However, these types of platforms required thick materials and very expensive elaboration techniques. As an alternative technology, InGaZnO (IGZO) thin film-PT structure has attracted a lot of interest in developing high-performance and low-cost optoelectronic devices due to their various advantages such as good chemical stability, low fabrication cost, excellent transistor properties, low-temperature processing, flexibility, low noise effects and good reliability [6, 7, 8, 9, 10]. Nevertheless, the main constraints limiting the use of IGZO-TFT in developing optoelectronic devices are the low generated photocurrent and spectrally limited responsivity, making it challenging for advanced optoelectronic applications. (see Table III. 1)

Table III.1. Overall performance comparison between the optimized IGZO mid-IR TF PT designs and several reported phototransistor designs based on III-V and II-VI compounds, Graphene, BP-based heterostructures.

Mid-IR sensor designs	**Sensing wavelength (µm)**	**I_{ON}/I_{OFF} ratio (dB)**	**Responsivity (A/W)**	**Detectivity (Jones)**	**Signal to noise ratio**	**Ref.**
GeSn IR photodiode	2	49	0.033	-	7.3×10^{3}	[139]
InAs/InAsSb superlattice	4.5	146	1.42	7×10^{11}	1.4×10^{4}	[140]
InAs/AlSb/ GaSb superlattice PT	3.6	-	1.9×10^{3}	1.1×10^{13}	-	[141]
nanostructured PbSe-based PT	3	36	90	2×10^{12}	4.2×10^{3}	[142]
Graphene/Si heterostructure	2.75	13.5	0.13	-	2×10^{3}	[143]
Graphene-Bi_2Se_3 Heterostructure	3.5	8.32	1.97	1.5×10^{11}	483	[146]
Photoconductor based on BP-Arsenic alloy	3.6	-	11.2	6×10^{10}	-	[147]

BP with interdigitated electrodes	2.5	12	0.047	-	1.8×10^{3}	[148]
BP/ SiO_2/Si heterostructure PT	2	-	8.5	1.7×10^{9}	-	[149]
BP/MoS_2 heterostructure photodiode	3.6	53.5	0.9	1.2×10^{10}	1.3×10^{4}	[150]
Au plasmons/Ge grating photodetector (PD)	1.55	12	0.38	-	398	[151]
Metal grating plasmons/Graphene PD	2.1	34	16.5	-	5×10^{3}	[152]
IGZO TF PT with BP capping layer	3.2	128	123	2.6×10^{14}	1.6×10^{5}	Our work
IGZO TF PT with Optimized BP/Au/BP sensitive film	3.2	166	388	6.9×10^{14}	2.2×10^{6}	Our work

Recently, broadband phototransistors have demonstrated superior performance for large light spectral optoelectronic-related applications, leading them to be considered more effective in different engineering fields, such as multispectral imaging, telecommunications, spectroscopy applications, environmental monitoring, biomedical sensing and chemical engineering [11, 12, 13]. Therefore, the development of new designs and techniques to improve the device photo-responsivity at broadband wavelength ranges is required. In this framework, stacking additional films on the IGZO channel using adequate materials to form a p-n structure can improve the photo-sensing spectrum and photoresponsivity as compared to that provided by the conventional phototransistors [13, 14, 15, 16, 17, 18]. Furthermore, various advanced materials such as MoS_2, graphene, 2D monolayers and Ge quantum dots were used to achieve high IR photocurrents [18, 19, 20]. However, the latter materials show degraded mid-IR photodetection characteristics. Basically, III-V and II-VI compounds, graphene-based heterostructures provide highly-detective sensors over the mid-IR spectrum range [21, 22, 23, 24, 25]. Despite this advantage, expensive growth methods, thermal reliability and dark noise effects constitutes the main limitations preventing the deployment of this mid-IR sensor technology for several practical applications [26,27]. Aiming at addressing these issues, researchers have turned out towards the exploration of alternative low-cost and effective mid-IR sensitive materials and technologies with low-processing complexity to be applied for the design of novel sensor architectures [26, 27, 28, 29, 30, 31, 32, 33, 34, 35]. Following this direction, black phosphorus (BP) has recently attracted research interest in widespread optoelectronic applications due to its unique electronic and optical properties such as direct narrow band gap, tunable mid-

IR photoresponse, and high charge carrier mobility [27]. Moreover, inserting an ultra-thin metallic layer (Au, Ag, Al,..) in the BP sensitive material can promote improved light management properties, thus leading potentially to achieve enhanced and extended mid-IR photoresponse. Intuitively, merging IGZO TFT technology with BP/Au/BP multilayered sensitive film can offer a great promise for designing high-performance, low dark noise and cost-effective mid-IR phototransistors. To the best of our knowledge, no design and elaboration approaches based on combining optimized BP sensitive layer with intermediate gold (Au) ultra-thin film and DFT-FDTD modeling were performed to develop high-performance broadband mid-IR IGZO thin-film phototransistors. Besides, only the visible optical properties have been carried out for bulk BP so far. In this work, the electronic and optical properties of bulk BP are investigated using accurate DFT computation within PBE-GGA and screened hybrid YS-PBE_0 functional taking into consideration van der Waals correction. Moreover, a new broadband Infrared IGZO TF PT based on optimized BP/Au/BP sensitive film is proposed and analyzed by developing DFT-FDTD numerical models combined with a PSO-based optimization technique. Using this new systematic investigation, the proposed approach offers exciting opportunities for designing high-performance mid-IR broadband optoelectronic devices.

III.2 Computational details

In this section, we present versatile computation frameworks for the design of new high-performance IGZO mid-IR TF PT based on BP capping layer and Au intermediate layer. The first objective relies on carrying out DFT calculations to predict the electronic and optical properties of buck BP material. In the second step, this section presents the adopted FDTD-based optical modeling and transport mechanism used to analyze the performance of the proposed IGZO mid-IR TF PT based on BP/Au/BP multilayered capping layer.

Fig.III. 1 shows the cross-sectional view of the proposed IGZO-capped BP/Au/BP mid-IR TF PT. The choice of the IGZO TFT platform is made taking into account its cost-effectiveness property as well as its ability for offering low dark noise effects. The device relies on introducing Au middle layer sandwiched between two black phosphorus thin-layers, forming an infrared sensing thin-film. The IGZO is capped with

BP/Au/BP thin film, which is separated from drain and source contacts, as it is described in Fig.III. 1, to avoid the current flow over the BP layer [38]. From the latter figure, t_{BP1} and t_{BP2} are respectively the thickness values of the top and bottom BP films, t_{Au} refers to the gold interlayer thickness, L refers to the channel length, t_{IGZO} is the thickness of the IGZO channel and tox represents the thickness of the SiO_2 gate dielectric.

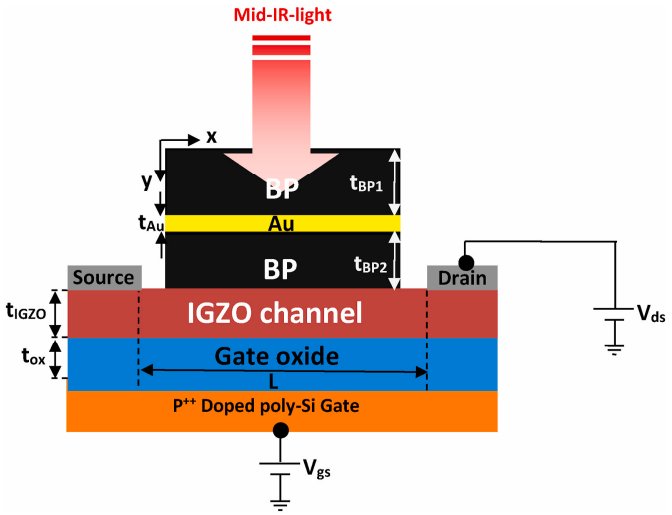

Fig. III.1. Cross-sectional view of the analyzed IGZO TF PT based on BP/Au/BP multilayer capping film.

In order to accurately analyze the device mid-IR sensing performances, the optical and electronic properties of the introduced black phosphorus should be determined. For this purpose, DFT calculations were carried out using the Perdew-Burke-Ernzerhof Generalized Gradient Approximation (PBE-GGA) combined with the screened hybrid ($YS\text{-}PBE_0$) functional to treat the exchange-correlation potential of interacting electrons [36,37]. The latter hybrid functional is regarded similar to the so-called Heyd-Scuseria-Ernzerh (HSE06) one, allowing the efficient prediction of semiconducting materials electronic properties due to its ability for taking into account electrons interaction [38]. As the BP layers basically are adhered with weak van der Waals forces, the Grimme's general dispersion correction termed DFT-D3 is utilized [39]. The simulation is implemented in the full-potential Wien2k code [40] with the projector augmented wave (PAW) pseudo-potentials. The initial BP orthorhombic structure for the DFT computation is shaped according to the experimental lattice constants in $\vec{a}$, $\vec{b}$, and $\vec{c}$, which are respectively given as 4.376 Å, 3.314 Å, and 10.478 Å, and the associated unit cell volume is 151.77 $Å^3$ [41]. The kinetic energy cutoff for

the plane-wave basis was fixed at 500 eV. To obtain the theoretical equilibrium crystal structure, the BP atomic structure was fully optimized with less than 0.1 eV/Å of force and 10^{-5} eV/atom of energy difference. The Brillouin zone is sampled using a $12 \times 12 \times 12$ k-point mesh for the band structure computation. Next, the bulk BP material electronic and optical properties are examined by extracting the band structure, band gap value, dielectric response function and the refractive indices. Therefore, the obtained electronic and optical parameters will be used for the numerical modeling of the investigated IGZO IR TF PT based on BP/Au/BP sensitive layer.

After estimating the electronic and optical parameters, the device is then modeled by using ATLAS 2-D and Luminous modules available in SILVACO software [42]. In this context, Finite-difference time-domain (FDTD) is used to model the photo-generation mechanism in the investigated structure by estimating the absorbance and reflectance optical parameters of the BP/Au/BP capping layer. The details regarding the FDTD method can be found in [43,44]. The optical factors are calculated using the following equations :

$$A(\lambda) = \frac{\int_V \frac{1}{2} \left|\vec{E}_y(\vec{r})\right|^2 \omega \varepsilon_0 \varepsilon_i''(\lambda) dV}{\int_S \frac{1}{2} \mathrm{Re}\left\{\vec{E}_y(\vec{r}) \times \vec{H}^*(\vec{r})\right\} dS} \quad \text{(III.1)}$$

$$R(\lambda) = \frac{\int_{port1} \left(E_{ci} - E_{1i}\right) E_{1i}^* dA_1}{\int_{port1} \left(E_{1i} E_{1i}^*\right) dA_1} = \frac{reflected\ power}{Incident\ power} \quad \text{(III.2)}$$

where, A denotes the absorbance, λ is the wavelength, ε_0 is the permittivity of the vacuum, ε_i'' denotes the wavelength-dependent complex dielectric function, which is taken from the obtained DFT results. Besides, E_y denotes the electric field in the vertical direction, $\vec{H}^*$ refers to the complex magnetic field conjugate, ω is the angular frequency. The reflectance coefficient (R) is defined as the ratio between reflected and incident powers as it is described in Eq IV.2, where E_{ci} is the electric field intensity at the port, which relies on the excitation added to the reflected field, E_{1i} represents the electric field pattern of the top port.

Thereafter, the device transport mechanism in the IGZO channel is modeled by using the drift-diffusion model with finite-element numerical technique available in the ATLAS-2D module [42], which enables self-consistently solving the Poisson and continuity equations represented by the following formulation

$$div(\varepsilon \nabla \psi) = -\rho \quad \text{(III.3)}$$

$$\rho = q\left(p - n + n_t - p_t - p_d + N_d\right) \quad \text{(III.4)}$$

$$\frac{1}{q} div(\vec{j}_n) - R_n + G_n = 0 \quad \text{(III.5)}$$

$$-\frac{1}{q} div(\vec{j}_p) - R_p + G_p = 0 \quad \text{(III.6)}$$

where ρ is the net charge density, ε is the absolute permittivity, q represents the electron charge, ψ is the electrostatic potential, N_d is the channel doping concentration, n_t and p_t refers to charged states of conduction and valence band tails (CBT, VBT), p_d is the shallow donor-like density approximated by using the model given in Ref [45]. The electron and hole current densities are represented by J_n and J_p respectively, while the associated generation and recombination rates are denoted respectively by G_n, G_p, R_n and R_p.

Importantly, the energy distribution of defect states in the band gap should be accounted due to the amorphous nature of the IGZO material [42, 45, 46, 47]. Moreover, tunneling models and Electric Field-Dependent Mobility are incorporated in the developed numerical model.

Aiming at assessing the accuracy of the developed numerical modeling methodology for the effective analysis of newly emerging IGZO TF PT based on capping the channel with appropriate sensitive film, the developed models should be validated by comparing the numerical results with the experimental ones. To the best of our knowledge, no experimental investigations reporting mid-IR IGZO TF PTs based on BP sensitive film. Therefore, the modeling process is applied the device based on Selenium (Se) capping layer and the material optical and electrical parameters are taken

from Ref. [48]. Fig.III. 2 shows I_{ds}-V_{gs} characteristics obtained from our developed model and that of the experimental data reported in Ref. [15]. It is demonstrated from this figure the capability of the developed model for correctly reproducing the experimental data, thus confirming the effectiveness of the presented numerical modeling methods. Despite this agreement, a slight difference between the numerical and experimental data is observed for gate voltages around -5V as it is shown in Fig.III. 2. This discrepancy can be attributed to the inability of the developed numerical model to take several effects related to the experimental conditions during the device elaboration, which can affect the diffusion current of the IGZO TFT in the off-state. These effects are mainly related to the deposition of the gate oxide and its uniformity, the surface recombination states in IGZO as well as defects induced by dislocation between the Selenium capping layer and IGZO channel. The mentioned experimental-related effects can generate parasite oxide capacitances, which influence the off-state current of the IGZO TFT device. Besides, the observed jitter for numerical data under darkness is correlated with the complexity of diffusion mechanism and charge transport properties, where it is extremely difficult to solve Poisson's and continuity equations when an amorphous IGZO channel is considered. This behavior is found consistent with several numerical investigations of IGZO TFTs [45,47].

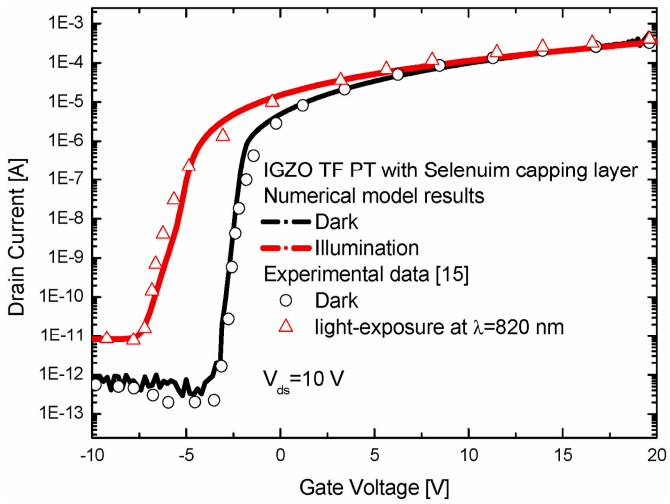

Fig. III.2. I_{ds}-V_{gs} curves of IGZO TF PTs under dark and illumination conditions obtained from the developed model and the experimental results [15] with λ = 820 nm, V_{ds} = 10 V, L = 150 µm, W = 1000 µm and t_{IGZO} = 20 nm.

III.3 Results and discussion

In this section, we start by discussing the relevance of the results investigating electronic and optical properties of bulk black phosphorus using DFT calculation. Key parameters involving the band gap value, dielectric function and the associated refractive indices over the mid-infrared range, crucial for the evaluation of BP sensing characteristics, are extracted and analyzed by combining YS-PBE_0 exchange-correlation hybrid functional with DFT-D3 van der Waals correction (YS-PBE_0+DFTD3). Subsequently, the obtained electronic and optical properties of BP are implemented in FDTD modeling framework to estimate the IR absorbance parameter, which will be applied to investigate the optoelectronic properties of the proposed IGZO IR TF PT based on BP/Au/BP multilayered capping film. The last step is dedicated to the optimization of the device structure using an effective metaheuristic technique based on Particle Swarm Optimization (PSO) iterative scheme.

III.3.1 DFT results

First-principles computations are carried out using combined PBE-GGA and YS-PBE_0 functionals with van der Waals (vdW) correction to achieve a good agreement with the experimental electronic properties of bulk BP. In this context, the atomic structure of BP in the orthorhombic phase with space group Cmca (No. 64) is described in Fig.III. 3 (a). Principally, atoms are coupled by strong covalent bonds along the orbitals shaped by sp3 hybridization, creating an orthorhombic lattice with puckered honeycomb structure. Besides, the (a and b) lattice constants are respectively directed to the zigzag and armchair directions (x and y-axis), while c is considered along the z-axis in the interlayer direction. The fully relaxed atomic structure is found highly reliable. The obtained (a, b) lattice constants after relaxation are close to the experimental ones, while c is only 0.15% larger than the measured one (c = 10.493 A). This slight discrepancy is attributed to the use of PBE-GGA approximation with the DFT-D3 van der Waals correction, which can slightly enlarge the c lattice parameter [48].

The band structure is an essential electronic property that should be analyzed for the design of materials appropriate for novel optoelectronic systems. It shows the correlation between electron wave and energy vectors. Accordingly, the electronic band

structure and Density of States (DOS) of bulk BP within PBE-GGA and YS-PBE_0 approaches including DFT-D3 van der Waals correction are calculated and depicted in Fig.III. 3 (c) and (d), respectively. The accompanying first Brillouin zone (BZ) is displayed in Fig.III. 3 (b). It can be seen that the conduction band minimum (CBM) and valence band maximum (VBM) are located at the high symmetry Z point, thus indicating the direct band gap nature of bulk BP with the value of 0.34 eV. Moreover, the semiconducting nature of bulk black phosphorus can be further be verified from the total DOS plot (Fig.III. 3 (d)), where the band gap is kept around the Fermi level. In addition, Fig.III. 3 (d) indicates the absence of extended states in the energy levels in the band gap. The calculated gap energy of BP is found in good agreement with the experimental one and consistent with previous first-principles investigations based on different functionals [49, 50, 51]. Therefore, the use of combined PBE-GGA + YS-PBE_0 approximations with DFT-D3 vdW correction can properly fit the electronic characteristics of the bulk BP.

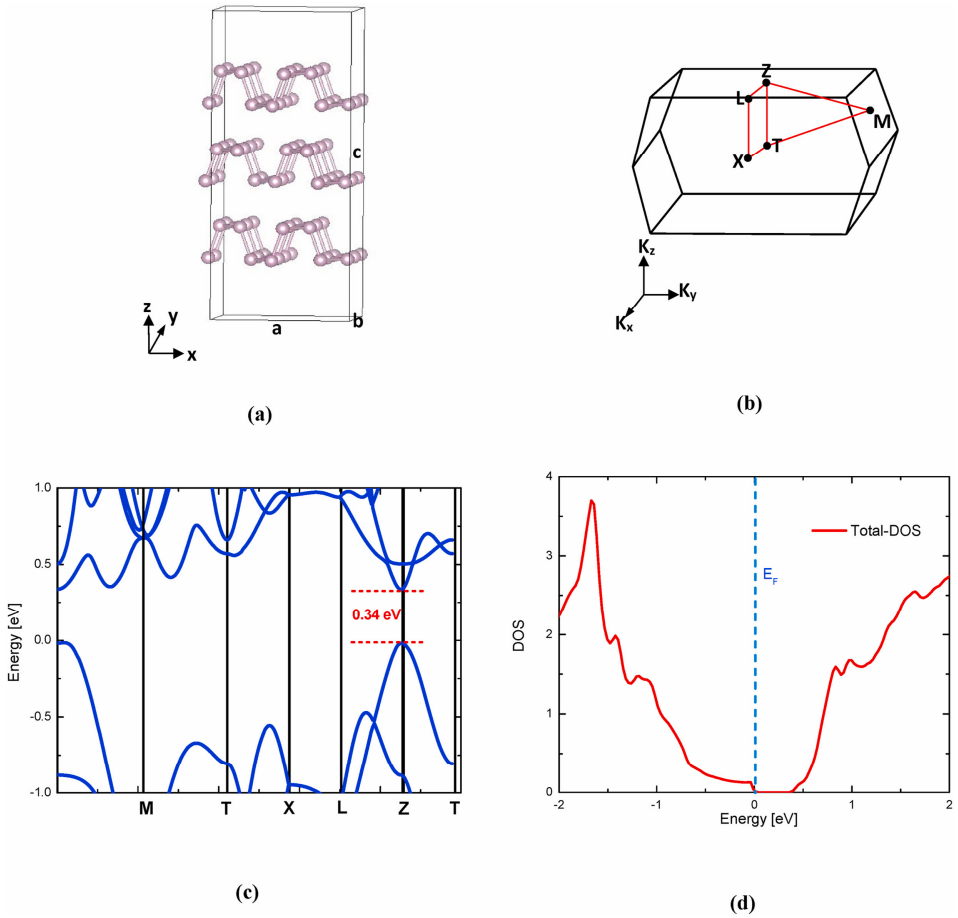

Fig. III.3. **(a)** Orthorhombic crystal structure of bulk BP. **(b)** Brillouin zone path of BP primitive cell. **(c)** Electronic band structure for bulk BP computed with using combined PBE-GGA and YS-PBE0 functionals with DFTD-3 van der Waals correction. **(d)** Density of states (DOS) of bulk BP.

The investigation of light-matter interaction is important for the study of optical sensor devices. Principally, semiconductors for IR sensing should exhibit high absorption and low reflection characteristics. To assess the appropriateness of bulk BP as a sensitive film for phototransistor devices, we study the main optical properties using PBE-GGA and YS-PBE_0 approaches. The real ($\varepsilon 1$) and imaginary (ε_2) parts of the dielectric function are plotted as a function of photon energy in Fig.III. 4 (a). It is revealed from this figure that the $\varepsilon 1$ of bulk BP increases with the photon energy increase to reach its maximum value at 4.9 eV. Besides, the static dielectric constant at zero frequency limit is 11.4. These high values are attributed to the small gap energy, where it is known that lower band gap materials yield larger dielectric values. Further, negative values for the real part of the dielectric function are observed for photon energy values superior to 6.2 eV, which can be explained by the metallic character of

intervals of the electromagnetic spectrum. On the other hand, it is observed from Fig.III. 4 (a) that the imaginary part exhibits rising followed by lowering tendencies with slight variations within the energy range of [4eV–6eV]. The highest peak of the imaginary part of the dielectric response function achieves 13.6.

The BP complex refractive index $N(\omega)=n(\omega)+ik(\omega)$ is extracted, where $n(\omega)$ represents the refraction index and $k(\omega)$ is the extinction coefficient. The latter are respectively displayed in Fig.III. 4 (b). It can be seen from this figure that high refractive index values around 4.1 are observed for mid-IR wavelengths. Fig.III. 4 (b) demonstrates that the extinction coefficient exhibits a pronounced step at an approximate wavelength value of $\lambda = 2.7$ μm, thus indicating the broadband absorption of BP over the mid-IR spectral range. This is mainly attributed to the low band gap energy of bulk BP material. Therefore, such electronic and optical properties of bulk black phosphorus make it highly attractive for IR optoelectronic applications. These outstanding characteristics inspire new insights for the design of novel high-performance IR sensors, which constitutes the main objective of the next sub-section.

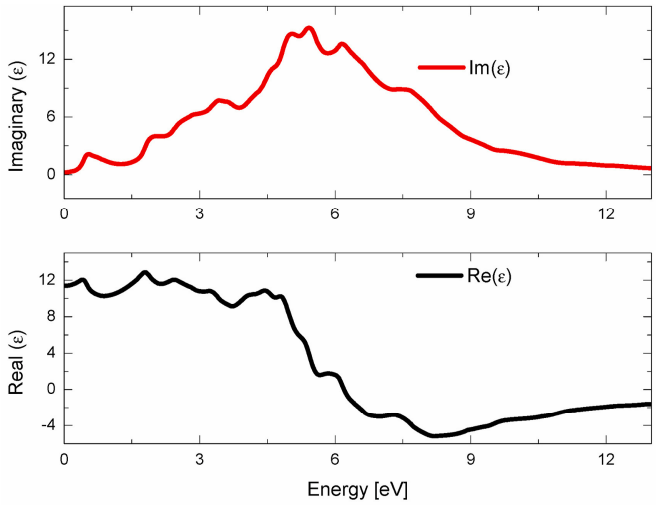

(a)

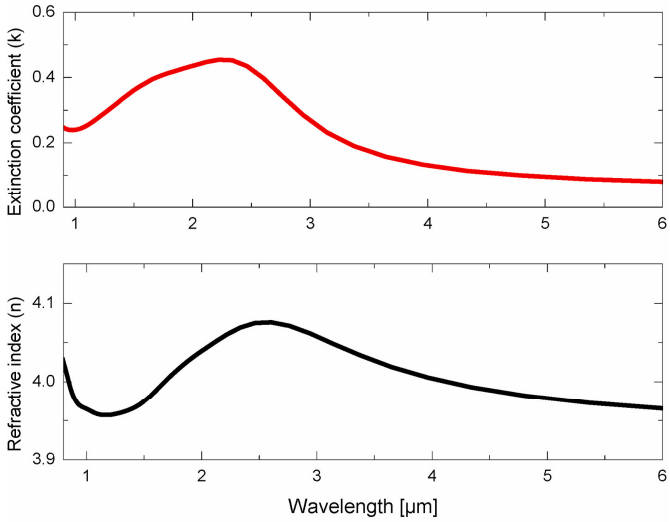

(b)

Fig. III.4. **(a)** Real and Imaginary parts of the dielectric function **(b)** Refractive index and extinction coefficient of bulk BP using DFT calculations based on PBE-GGA and YS-PBE0 functionals with DFT-D3 van der Waals correction.

III.3.2 Broadband mid-IR BP IGZO phototransistor design

To analyze the performance of the proposed BP phototransistor design, the obtained electronic and optical parameters as it is outlined in the last sub-section are introduced in the numerical model procedure presented in the computation details. The IGZO channel of the TF PT is capped with a BP layer, acting as a mid-IR absorbing film. The associated I_{ds}-V_{gs} are calculated under dark and IR (2 μm) light-exposure conditions and

depicted in Fig.III. 5 with V_{ds} = 10 V, t_{ox} = 80 nm, t_{BP} = 180 nm and t_{IGZO} = 20 nm. The latter figure shows that by capping the IGZO channel with BP sensitive layer, the device demonstrates a good infrared photoresponse. This is because of the ability of BP for absorbing mid-IR light matching well with its band-gap energy (0.34 eV) and creating e/h pairs, which will be driven to the back IGZO channel. These photo-excited carriers form a back channel current path and thereby induce a threshold voltage shift to negative values. This effect gives rise to an important photocurrent at low gate bias, when an applied drain-to-source voltage is considered. Besides, the proposed mid-IR phototransistor exhibits an ultralow OFF current, which is due to the use of the IGZO TFT platform known to offer a very low leakage current.

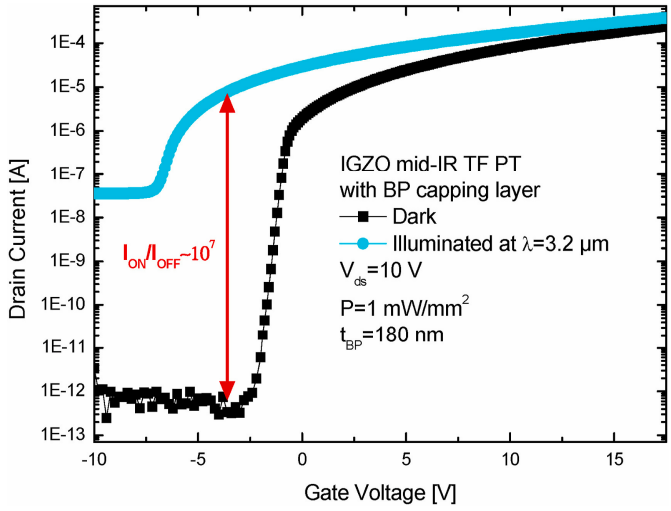

Fig. III.5. Ids-Vgs transfer characteristics of IGZO mid-IR TF PTs based on BP thin-film capping layer with tBP = 180 nm, tox = 80 nm and tIGZO = 20 nm, Vds = 10 V, L = 100 μm, W = 1000 μm and Pi = 1 mW/mm2.

Although the good mid-IR photoresponse characteristics associated with the IGZO TF PT based on BP capping layer, the device photodetection capability is still far from that expected for several emerging applications. Further improvements should be achieved for the development of high-performance sensors. Basically, mid-IR sensors commonly suffer from the low responsivity, which is attributed in a large extent to certain imperfections related to the trade-off between absorbance and anti-reflection capabilities of sensitive layers within this specific spectral band. Aiming at boosting up the device performance, Au intermediate ultra-thin film is introduced in the BP sensitive layer, which is expected to further enhance the device IR photoresponse. In addition, the

position of the Au ultrathin film within BP thin-film plays a crucial role in modulating the optical behavior of the sensitive capping layer, which can in turn influence the phototransistor mid-IR photodetection properties. Accordingly, the geometry of the introduced BP/Au/BP multilayer is optimized using the PSO-based metaheuristic technique, where the objective function should satisfy the high absorbance capability of the structure over the mid-IR spectral range. The exploited PSO optimization approach, proposed by Eberhart and Kennedy [52], is naturally inspired and is a subfamily of evolutionary, population-based algorithms for which the basic idea is to mimic the concept of bird flocking social behavior. It enables achieving the global solution of complex optimization problems within a low computation time using an iterative process of generations. PSO has been exploited in a variety of disciplines to optimize a set of parameters of multi-dimensional and nonlinear functions, specifically showing a great promise for solving complex microelectronic and optoelectronic optimization problems [52, 53, 54]. This is thanks to its fascinating benefits like versatility, effectiveness, and simple implementation. In fact, PSO executes searching by moving the particles around the defined search space with respect to the introduced fitness function. The swarm is composed of particles for which their position (X_i^k) and velocity (V_i^k) are iteratively updated using the following formulas

$$V_i^{k+1} = wV_i^k + c_1 r_1^k (P_{li}^k - X_i^k) + c_2 r_2^k (P_{gi}^k - X_i^k) \quad \text{(III.7-a)}$$

$$X_i^{k+1} = X_i^k + V_i^{k+1} \quad \text{with } i = 1..m \quad \text{(III.7-b)}$$

where w is the inertia weight, m refers to the swarm size, c_1 and c_2 denote the cognitive and social acceleration factors; r_1 and r_2 are random numbers, particle best position and best position of the particles group are respectively denoted by P_{li}^k and P_{gi}^k.

It is important to note that more details concerning the introduced PSO-based metaheuristic technique can be found in [54]. Therefore, the objective function related to the enhancement of BP/Au/BP mid-IR absorbance is considered, which can be represented by the following formula

$$F(X) = \frac{1}{A(\lambda = 3.2\mu m)} \quad \text{(III.8)}$$

where X is the design variables vector given by: $X= (t_{BP1}, t_{BP2}, t_{Au})$, A (λ=3.2 µm) represents the absorbance of BP/Au/BP multilayered mid-IR sensitive layer, which is calculated using the FDTD-based methodology outlined in section. III.2. Prior to the optimization procedure, the applied gate and drain voltages are fixed at -1V and 10 V, respectively. Besides, in order to be very close to the technology node of IGZO TFTs [15], the device structure is considered with 80 nm of oxide thickness, 20 nm of IGZO thin-film thickness, channel length and width of 100 µm and1000 µm, respectively. Each design parameter of the defined X vector is confined in a given range $x \in [x_{i\min}, x_{i\max}]$ with $x_i \in X$.

Fig.III. 6 depicts the evolution of the fitness function against the generation number of the PSO procedure. Clearly, the objective function (Eq. (8)) is minimized thereby the mid-IR absorbance of BP/Au/BP multilayered structure is maximized. It can be also observed that an excellent stabilization is achieved around 340 generations. Accordingly, the optimized design parameter vector is given by X= (147 nm, 43 nm, 16 nm), which correlates with the maximum absorbance value over the mid-IR range. The I_{ds}-V_{gs} transfer curves of the optimized IGZO mid-IR TF PT based on BP/Au/BP multilayered capping layer under dark and light exposure conditions are shown in Fig.III. 7 (a). This figure demonstrates the superior photocurrent and a very large threshold voltage shift to negative values of the optimized device. This outstanding photoresponse in a wide operating voltage window is attributed to the use of Au noble metal and the optimization approach, which promoted exciting opportunities to achieve efficient optical coupling between mid-IR light and plasmons. Moreover, the use of multilayer structure promotes enhanced light management leading to improve the structure light-scattering effects. These effects have together contributed to the enhancement of BP capping film absorbance behavior over the mid-IR range. To confirm this hypothesis, Fig.III. 7 (b) shows the mid-IR absorbance spectra of BP (t_{BP} = 180 nm), BP (t_{BP1} = 90 nm)/Au (t_{Au} = 10 nm)/BP (t_{BP2} = 90 nm), the optimized BP (t_{BP1} = 147 nm)/Au (t_{Au} = 16 nm)/BP (t_{BP2} = 43 nm), and 180 nm thick Germanium thin-films as the commonly used material for IR sensing applications. The BP-based sensitive layers exhibit higher absorption capabilities of mid-IR light, which is beyond the limit of Germanium. This is ascribed to the suitably matched band-

gap energy of BP (0.34 eV) for mid-IR photodetection as compared to that of the Germanium material (0.67 eV). It can be also noticed from Fig.III. 7 (b) that the use of multilayer structure with Au intermediate ultrathin film boosts the BP absorbance behavior. More importantly, the optimized structure demonstrates broadband and strong mid-IR absorbance (A_{max} = 92%) as compared to other structures. This benefit opens up a new pathway for extending the operation of the investigated BP-based mid-IR sensor into a longer wavelength range, thus significantly enhancing its functionalities. These outstanding results can be explained by the role of the adopted optimization strategy for the identification of the best BP/Au/BP geometry, which promotes improved light-scattering effects. Fig.III. 7 (c) illustrates the electric field distribution in the optimized structure and the conventional BP film at the wavelength value of 3.2 µm. These electric field profiles can consolidate the aforementioned explanations, where the optimized BP/Au/BP structure shows highly confined electric field with densities within the investigated sensitive layer, as compared to that of the BP film. This indicates the enhanced light trapping capability of the optimized BP/Au/BP multilayered capping film as compared to the conventional 180 nm thick BP layer.

For the completeness of this work, the device Figure of Merits (FoMs) parameters including Responsivity, Detectivity, signal to noise ratio and I_{ON}/I_{OFF} ratio are calculated for the optimized IGZO mid-IR TF PT based on BP/Au/BP multilayer capping film and compared with mid-IR sensors reported in the literature [22, 23, 24, 25, 26, 29, 30, 31, 32, 33, 34, 35]. The optimized device greatly outperforms the developed mid-IR photosensors in terms of FoMs parameters, yielding a giant responsivity of 388 A/W and over than 2 × 106 of dark noise ratio. This proves its high photodetection capabilities and low power consumption property. In addition, the optimized device demonstrates enhanced photoresponse characteristics as compared to photodetectors based on plasmonic and combined 2-D material with metal grating structures [34, 35]. This is attributed to the optimization technique and the use of IGZO TFT platform, leading to achieve enhanced photoresponse characteristics.

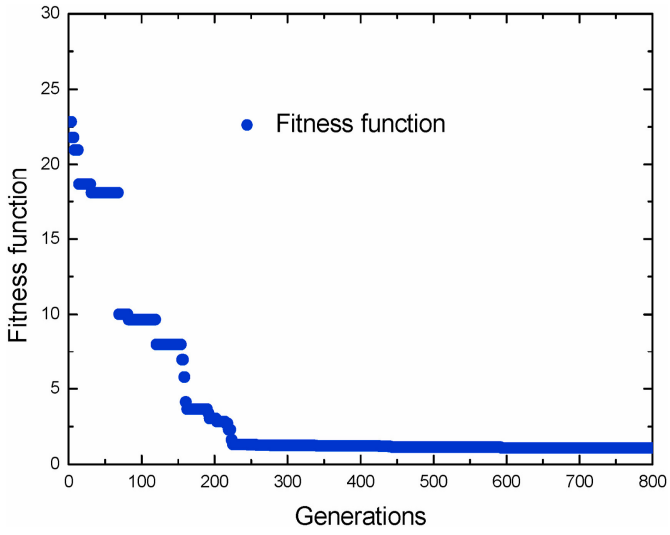

Fig. III.6. Fitness functions against generation number of PSO computation.

The optimized design structure can be fabricated following several fabrication steps. In this context, the IGZO thin-film can be deposited on SiO_2/Si substrate using Radio Frequency (RF) Sputtering method, where the targets composition can be taken with In_2O_3:Ga_2O_3:ZnO = 1:1:1 mol% [9,10,15]. Thereafter, the source and drain electrodes can be realized by thermal evaporation technique and photolithography using an appropriate shadow mask. Then, the BP top and bottom films with optimized thickness values can be deposited by short-distance transport (SDT) method using a uniform temperature [55]. On the other hand, the intermediate gold thin-film can be grown by thermal evaporation technique. Some challenges for the fabrication of the optimized device can be encountered, which are mainly related to the uniformity and thickness accuracy of the introduced gold metallic layers and BP top and bottom films. Therefore, the experimental fabrication of the optimized IGZO mid-IR TF PT based on BP/Au/BP multilayered structure is considered as a perspective of this work, where the use of appropriate experimental facilities and characterization techniques to elaborate this kind of IR phototransistor is crucial.

Considering these significant benefits, the proposed systematic investigation framework based on the strategic combination between DFT formalism, FDTD optical modeling and PSO metaheuristic technique is believed to offer new insights for designing alternative high-responsivity, cost-effective and low dark noise mid-IR phototransistors suitable for the emerging optoelectronic applications.

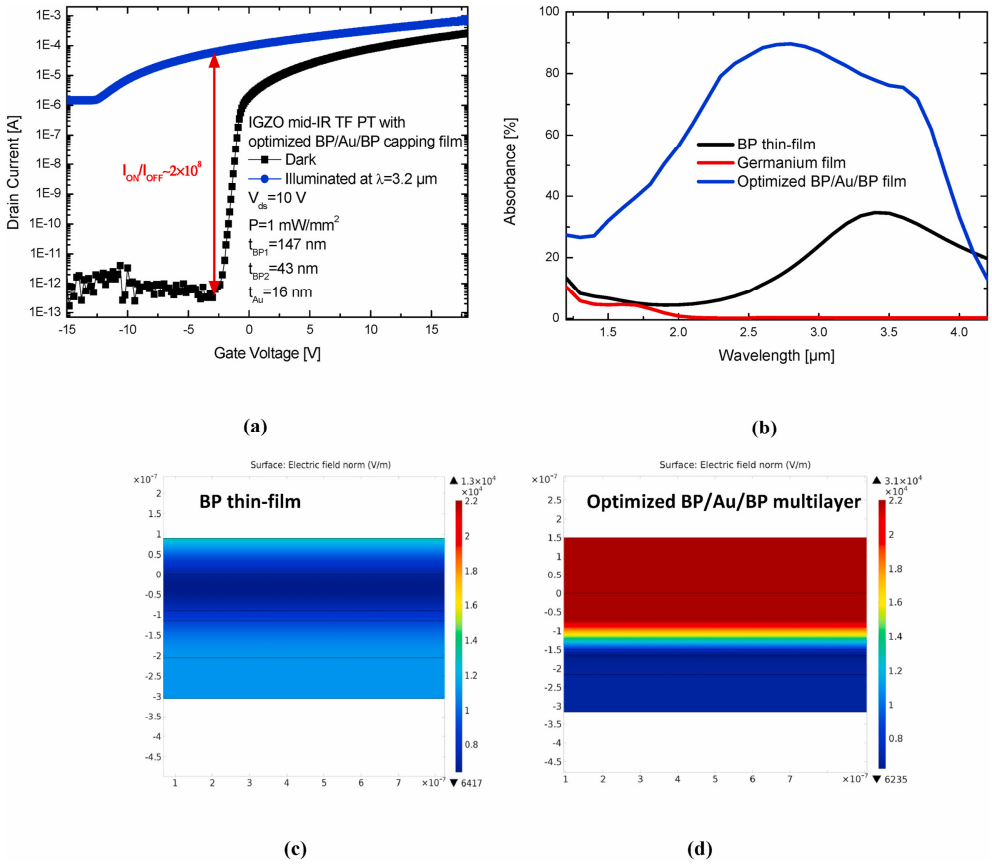

Fig. III.7. **(a)** I_{ds}-V_{gs} transfer curves of the IGZO mid-IR TF PTs based on optimized BP/Au/BP sensitive film with t_{BP1} = 147 nm, t_{BP2} = 43 nm, t_{Au} = 16 nm, V_{ds} = 10 V, L = 100 µm, W = 1000 µm, t_{ox} = 80 nm and t_{IGZO} = 20 nm. **(b)** Mid-IR absorbance spectra of BP thin-film, 180 nm thick Germanium layer, Optimized BP/Au/BP multilayered structure. **(c)** Electric field distribution within 180 nm thick BP and the optimized BP/Au/BP tri-layer.

III.4. Conclusion

In this chapter, a novel broadband mid-IR IGZO TF PT based on both Black Phosphorus capping layer incorporating intermediate gold ultrathin-film is proposed. The optical and electronic properties of the Black Phosphorus are carried out using DFT computations that include PBE-GGA and YS-PBE0 functionals with DFT-D3 van der Waals correction. The absorbance of the BP sensing layer including intermediate gold ultra-thin film is performed using FDTD-based numerical modeling frameworks. To boost up the absorbance performance of the BP/Au/BP sensing layer, we combined FDTD modeling and PSO optimization technique which permits achieving near-perfect broadband mid-IR absorbance beahvior. It is found that the optimized BP/Au/BP capping film can extend the device photoresponse within the mid-IR spectral range, offering a high ION/IOFF current ratio of 166 dB, high responsivity exceeding 380

A/W and superior detectivity of 6.9×1014 Jones over a wide operating voltage window. Considering these significant performances, the proposed approach is expected to provide a valuable guideline the development of highly sensitive broadband photosensors.

References

[1] A.H. Atabaki, et al, Integrating photonics with silicon nanoelectronics for the next generation of systems on a chip Nat, Photonics, 556 (2018), pp. 349-354.

[2] C. Sun, et al, Single-chip microprocessor that communicates directly using light, Nature, 528 (2015), pp. 534-538.

[3] L. Colace, V. Sorianello, S. Rajamani, Investigation of static and dynamic characteristics of optically controlled field effect transistors, J. Lightwave Technol., 32 (2014), pp. 2233-2239.

[4] H. Ferhati, F. Djeffal, Boosting the optical performance and commutation speed of phototransistor using SiGe/Si/Ge tunneling structure, Mater. Res. Express, 5 (2018), p. 65902.

[5] C. Wang, Xi Zhang, W. Hu, Organic photodiodes and phototransistors toward infrared detection: materials, devices, and applications, Chem. Soc. Rev., 49 (2020), pp. 653-670

[6] X. Liu, et al, Transparent, high-performance thin-film transistors with an InGaZnO/aligned-SnO2-nanowire composite and their application in photodetectors; Adv. Mater., 26 (2014), pp. 7399-7404

[7] H. Ferhati, F. Djeffal, Giant responsivity of a new InGaZnO ultraviolet thin-film phototransistor based on combined dual gate engineering and surface decorated Ag nanoparticles aspects, Sensor Actuator Phys., 318 (2021), p. 112523

[8] Y. Zhai, G. Chen, J. Ji, Z. Wu, Y. Li, Q. Wang, Investigation of photocurrent transient variation in Au nanoparticles decorated IGZO phototransistor, Phys. E Low-dimens. Syst. Nanostruct., 113 (2019), pp. 92-96

[9] H. Yu, X. Liu, L. Yan, T. Zou, H. Yang, C. Liu, S. Zhang, H. Zhou, Enhanced UV-visible detection of InGaZnO phototransistors via CsPbBr3 quantum dots, Semicond. Sci. Technol., 34 (2019), p. 25013

[10] S.W. Pak, D. Chu, D.Y. Song, S.K. Lee, E.K. Kim, Enhancement of near-infrared detectability from InGaZnO thin film transistor with MoS2 light absorbing layer, Nanotechnology, 28 (2017), p. 475206

[11] X.-L. Wang, Y. Shao, X. Wu, M.-N. Zhang, L. Li, W.-J. Liu, D.W. Zhang, S.-J. Ding, Light response behaviors of amorphous In–Ga–Zn–O thin-film transistors via in situ interfacial hydrogen doping modulation, RSC Adv., 10 (2020), p. 3572

[12] Z. Zheng, L. Gan, J. Zhang, F. Zhuge, T. Zhai, An enhanced UV–Vis–NIR and flexible photodetector based on electrospun ZnO nanowire array/PbS quantum dots film heterostructure, Adv. Sci., 4 (2017), p. 1600316

[13] M.S. Mahdi, K. Ibrahim, N.M. Ahmed, A. Hmood, F.I. Mustafa, S.A. Azzez, M. Bououdina, High performance and low-cost UV–Visible–NIR photodetector based on tin sulphide nanostructures, J. Alloys Compd., 735 (2018), pp. 2256-2262

[14] H.-J. Na, N.-K. Cho, J. Park, S.-E. Lee, E.G. Lee, C. Im, Y.S. Kim, A visible light detector based on a heterojunction phototransistor with a highly stable

inorganic CsPbIxBr3-x perovskite and In–Ga–Zn–O semiconductor double-layer, J. Mater. Chem. C, 7 (2019), p. 14223

[15] H. Yoo, et al, High photosensitive Indium−Gallium−Zinc oxide thin-film phototransistor with a Selenium capping layer for visible-light detection, ACS Appl. Mater. Interfaces, 12 (2020), pp. 10673-10680

[16] J. Yang, H. Kwak, Y. Lee, Y.-S. Kang, M.-H. Cho, J.H. Cho, Y.-H. Kim, S. J. Jeong, S. Park, H.-J. Lee, H. Kim, MoS2–InGaZnO heterojunction phototransistors with broad spectral responsivity, ACS Appl. Mater. Interfaces, 8 (2016), pp. 8576-8582

[17] S. Wei, F. Wang, X. Zou, L. Wang, C. Liu, X. Liu, W. Hu, Z. Fan, J.C. Ho, L. Li ao,
Flexible quasi-2D perovskite/IGZO phototransistors for ultrasensitive and broadband
photodetection, Adv. Mater., 32 (2020), p. 1907527

[18] D.K. Hwang, et al, Ultrasensitive PbS quantum-dot-sensitized InGaZnO hybrid photo-inverter for near-infrared detection and imaging with high photogain, NPG Asia Mater., 8 (2016), p. 233

[19] H. Ferhati, F. Djeffal, L.B. Drissi, Enhanced infrared photoresponse of a new InGaZnO TFT based on Ge capping layer and high-k dielectric material, Superlattice. Microst., 156 (2021), p. 106967

[20] Z. Pei, H. Lai, J. Wang, W. Chiang, C. Chen, High-responsivity and high-sensitivity graphene dots/a-IGZO thin-film phototransistor, IEEE Electron. Device Lett., 36 (2015), pp. 44-46

[21] X. Ling, H. Wang, S. Huang, F. Xia, M.S. Dresselhaus, The renaissance of black phosphorus, Proc. Natl. Acad. Sci. U.S.A., 112 (2015), pp. 4523-4530

[22] P. Scajev, et al, Extension of spectral sensitivity of GeSn IR photodiode after laser annealing, Appl. Surf. Sci., 555 (2021), p. 149711

[23] D. Wu, J. Li, A. Dehzangi, M. Razeghi, High performance InAs/InAsSb Type-II superlattice mid-wavelength infrared photodetectors with double barrier, Infrared Phys. Technol., 109 (2020), p. 103439

[24] A. Haddadi, S. Adhikary, A. Dehzangi, M. Razeghi, Mid-wavelength infrared heterojunction phototransistors based on type-II InAs/AlSb/GaSb superlattices, Appl. Phys. Lett., 109 (2016), p. 21107

[25] A. Motmaen, A. Rostami, S. Matloub, Ultra high-efficiency integrated mid infrared to visible up-conversion system, Sci. Rep., 10 (2020), p. 9325

[26] X. Wang, Z. Cheng, K. Xu, H.K. Tsang, J.-B. Xu, High-responsivity graphene/silicon-heterostructure waveguide photodetectors, Nat. Photonics, 7 (2013), pp. 888-891

[27] J. Kim, et al, Graphene-based mid-infrared photodetectors using metamaterials and related concepts, ACS Photonics, 4 (2017), pp. 482-488

[28] L. Huang, K.-W. Ang, Black phosphorus photonics toward on-chip applications, Appl. Phys. Rev., 7 (2020), p. 31302

[29] M. Ye, J. Zha, C. Tan, K.B. Crozier, Highly sensitive, gate-tunable, room-temperature mid-infrared photodetection based on Graphene−Bi2Se3 heterostructure, Appl. Phys. Rev., 8 (2021), p. 31303
[30] M. Amani, E. Regan, J. Bullock, G.H. Ahn, A. Javey, Mid-wave infrared photoconductors based on black phosphorus-arsenic alloys, ACS Nano, 11 (2017), pp. 11724-11731
[31] M. Xu, Y. Gu, R. Peng, N. Youngblood, M. Li, Black phosphorus mid-infrared photodetectors, Appl. Phys. B, 123 (2017), pp. 123-130
[32] L. Huang, W.C. Tan, L. Wang, B. Dong, C. Lee, K.-W. Ang, Infrared black phosphorus phototransistor with tunable responsivity and low noise equivalent power, ACS Appl. Mater. Interfaces, 41 (2017), pp. 36130-36136
[33] J. Bullock, et al, Polarization-resolved black phosphorus/molybdenum disulfide mid-wave infrared photodiodes with high detectivity at room temperature, Nat. Photonics, 12 (2018), pp. 601-607
[34] L. Wang, et al, High-performance infrared Ge-based plasmonic photodetector enhanced by dual absorption mechanism, APL Photon., 5 (2020), p. 96104
[35] E. Khosravian, H.R. Mashayekhi, A. Farmani, Highly polarization-sensitive, broadband, low dark current, high responsivity graphene-based photodetector utilizing a metal nano-grating at telecommunication wavelengths, J. Opt. Soc. Am. B, 38 (2021), pp. 1192-1199
[36] J.P. Perdew, K. Burke, M. Ernzerhof, Generalized gradient approximation made simple, Phys. Rev. Lett., 77 (1996), p. 3865
[37] F. Tran, P. Blaha, Implementation of screened hybrid functionals based on the Yukawa potential within the LAPW basis set, Phys. Rev. B, 83 (2011), p. 235118
[38] J. Heyd, G.E. Scuseria, Efficient hybrid density functional calculations in solids: assessment of the Heyd–Scuseria–Ernzerhof screened Coulomb hybrid functional, J. Chem. Phys., 121 (2004), pp. 1187-1192
[39] S. Grimme, J. Antony, S. Ehrlich, H. Krieg, A consistent and accurate ab initio parametrization of density functional dispersion correction (DFT-D) for the 94 elements H-Pu, J. Chem. Phys., 132 (2010), p. 154104
[40] K. Schwarz, P. Blaha, G.K. Madsen, Electronic structure calculations of solids using the WIEN2k package for material sciences, Comput. Phys. Commun., 147 (2002), pp. 71-76
[41] R. Wyckoff, Crystal Structures, John Wiley, New York (1963)
[42] Atlas User's Manual, SILVACO TCAD (2012)
[43] H. Ferhati, F. Djeffal, Role of optimized grooves surface -textured front glass in improving TiO2 thin film UV photodetector performance, IEEE Sensor. J., 16 (2016), pp. 5618-5624
[44] F. Srairi, F. Djeffal, H. Ferhati, Efficiency increase of hybrid organic/inorganic solar cells with optimized interface grating morphology for improved light trapping, Optik, 130 (2017), pp. 1092-1098

[45] M. Adaika, Af Meftah, N. Sengouga, M. Henini, Numerical simulation of bias and photo stress on indium–gallium–zinc-oxide thin film transistors, Vacuum, 120 (2015), pp. 59-67

[46] J. Park, D.-K. Kim, J.-I. Park, I.M. Kang, J. Jang, H. Kim, P. Lang, J.-H. Bae, Numerical analysis on effective mass and traps density dependence of electrical characteristics of a-IGZO thin-film transistors, Electronics, 9 (2020), p. 119

[47] T.E. Taouririt, A. Meftah, N. Sengouga, M. Adaika, S. Chala, A. Meftah, Effects of high-k gate dielectrics on the electrical performance and reliability of an amorphous indium–tin–zinc–oxide thin film transistor (a-ITZO TFT): an analytical survey, Nanoscale, 11 (2019), p. 23459

[48] T.K. Todorov, S. Singh, D.M. Bishop, O. Gunawan, Y.S. Lee, T.S. Gershon, K. W. Brew, P.D. Antunez, R. Haight, Ultrathin high band gap solar cells with improved efficiencies from the world's oldest photovoltaic material, Nature communication, 8 (2017), p. 682

[49] Yi-Chia Tsai, et al, Contact engineering of trilayer black phosphorus with scandium and gold, IEEE J. Electron Devices Soc., 7 (2019), pp. 322-328

[50] P.-L. Gong, et al, Hydrostatic pressure induced three-dimensional Dirac semimetal in black phosphorus, Phys. Rev. B, 93 (2016), p. 195434

[51] J. Qiao1, X. Kong, Z.-X. Hu, F. Yang, W. Ji, Few-layer black phosphorus: emerging 2D semiconductor with high anisotropic carrier mobility and linear dichroism, Nat. Commun, 5 (2014), p. 4475

[52] M. Clerc, Kennedy, The particle swarm - explosion, stability, and convergence in a multidimensional complex space, J. IEEE Trans. Evolut. Comput., 73 (2002), pp. 6-58

[53] F. Djeffal, T. Bendib, R. Benzid, A. Benhaya, An approach based on particle swarm computation to study the nanoscale DG MOSFET-based circuits, Turk. J. Electr. Eng. Comput. Sci., 18 (2010), pp. 988-992

[54] H. Ferhati, F. Djeffal, A. Benhaya, Optimized high-performance ITO/Ag/ITO multilayer transparent electrode deposited by RF magnetron sputtering, Superlattice. Microst., 129 (2019), pp. 176-184

[55] M. Liu, S. Feng, Y. Hou, S. Zhao, L. Tang, J. Liu, F. Wang, B. Liu, High yield growth and doping of black phosphorus with tunable electronic properties, Mater. Today, 36 (2020), pp. 91-101

Chapter IV

Broadband Mid-IR graphene-phototransistor using strained black phosphorus sensing gate

***Abstract:** In this work, a new high-performance broadband Infrared Optically Controlled Graphene Field-Effect Transistor (IR–OC–GFET) using strained black phosphorus sensing gate is proposed and investigated. It is found that the proposed device with strained sensing gate provides enhanced optical performances over the middle infrared (Mid-IR) spectral band, making it a new potential alternative photoreceiver for chip-level optical communications.*

IV.1 Introduction

During the last few years, middle infrared (Mid-IR) phototransistors (PTs) play an important role in various emerging engineering systems including biosensing, optical wireless communication devices, thermal imaging, chemical detection and analysis, astronomy, spectroscopy applications, and security systems [1, 2, 3, 4]. In order to achieve high photoresponsivity performance over different spectral ranges, Numerous PT designs and models were developed using different approaches and technology platforms such as CMOS, organic transistors, tunneling-FET, multi-gate and thin-film transistors (TFT) [4, 5, 6, 7, 8, 9, 10, 11, 12, 13]. As an alternative technology, optically controlled field effect transistors (OCFETs) have gained extensive attention in developing high performance phototransistors due to their various advantages such as CMOS technology compatibility, high-sensitivity and excellent gate controllability [14]. However, the main limitations restricting the use of OCFET designs in developing optoelectronic devices are the low and spectrally limited photoresponsivity and the inherently limited drain photocurrent. These shortcomings make the conventional silicon-channel-based phototransistors challenging for advanced optoelectronic applications. Therefore, the development of new OCFET structures by including new channel and sensing gate materials to improve the device photoresponsivity at broadband Mid-IR wavelengths is required. In this framework, the rise of graphene two-dimensional (2D) material has attracted great interest for developing high-performance optoelectronic devices [15, 16, 17, 18, 19]. This is mainly due to the exceptional structural and optoelectronic properties provided by the graphene such as excellent electrical conductivity, flexibility, high-transparency and ultra-high carrier mobility [15,16]. Despite these properties, several optoelectronic limitations like low absorption capability and relatively narrow band photoresponsivity remain to be addressed for further improvement of the graphene-based photodetector performances [20, 21]. In this context, it is therefore essential to develop new approaches to fully use the electronic properties of graphene in order to enhance the derived photocurrent, while ensuring an improved gate photosensitivity. Therefore, a better understanding of sensor photodetection and electron transport mechanisms can provide new insights to develop high-performance broadband IR-phototransistor using single photosensitive bulk material.

Recently, black phosphorus (BP) material has attracted a great research interest in widespread optoelectronic applications due to its suitable electronic and optical properties such as direct and tunable band gap from near to far infrared region, and high charge carrier mobility [22, 23, 24, 25, 26]. These advantages make the BP material a potential alternative for bridging the gap of the optical sensing between near and far infrared spectral ranges for broadband IR optoelectronic applications [26]. Moreover, the absence of dangling bonds in the BP thin-film surface allows avoiding lattice mismatch issues, making it reliable and compatible with CMOS processing technologies [27]. In spite of interesting optical and electrical properties exhibited by the BP, further efforts should be devoted to BP-based photosensors to improve their performances and extend the sensing capability to higher wavelengths (middle and far IR). In other words, the total absorbance of BP thin-film over the Infrared spectral range is still relatively low and requires further enhancements, which is regarded as ongoing quests in current research in the field of optoelectronics. Consequently, new approaches should be developed to enhance the optical performances of BP thin-film for broadband infrared photodetection applications. Intuitively, the introduction of hydrostatic pressure on BP thin-film material can induce significant improvements in terms of structural, electrical and optical properties [27]. Following this direction, the main objective of this work is to exploit the high-performance properties of graphene and strained BP materials in order to develop an efficient broadband Mid-IR phototransistor [54]. The drain current is calculated by solving the Schrödinger equation using non-equilibrium Green's function (NEGF) formalism self-consistently coupled with 2D-Poisson equation. The role of strained BP sensing gate in enhancing the broadband IR OC-GFET performance is demonstrated. Therefore, combining strained BP sensing gate with graphene-channel material offers exciting opportunities for designing high-performance mid-IR broadband optoelectronic devices.

IV.2 Modeling frameworks

In this section, versatile modeling frameworks for the design and modeling of new high-performance graphene-nanoribbon infrared phototransistor (GNR IR PT) based on strained BP photosensitive gate are presented. The first objective is linked to carrying out first-principles calculations using DFT method to predict the electronic and optical properties of bulk BP material with and without pressure effects. In the second step, this

section presents the FDTD-based optical modeling used to estimate the IR absorbance behavior of the proposed BP under strain effects. The last step is dedicated to the IR–OC–GFET numerical modeling based on solving the Schrödinger/Poisson equations self-consistently using NEGF formalism.

IV.2.1 DFT computations

In order to analyze the role of strain effects on the IR photodetection properties of BP thin-film, we investigate its electronic and optical characteristics with and without pressure effects. To do so, full-potential Wien2k code with the projector augmented wave (PAW) pseudo-potentials is used [26]. The exchange-correlation potential of interacting electrons in BP under pressure conditions is studied by performing DFT calculations for which the Perdew-Burke-Ernzerhof Generalized Gradient Approximation (PBE-GGA) and the screened hybrid (YS-PBE0) functional, similar to the so-called Heyd-Scuseria-Ernzerh (HSE06), are considered [27, 28, 29]. The latter functional is considered efficient, been able to take into account electrons interaction, thus providing a correct prediction of the electronic characteristics associated with dissimilar semiconducting materials [30]. Importantly, the Grimme's general dispersion correction termed DFT-D3 is utilized to consider van der Waals forces induced between BP monolayers [31]. The initial BP structure for the DFT computation is shaped according to the experimental lattice constants in $\vec{a}$, $\vec{b}$, and $\vec{c}$, which are respectively given as 4.376 Å, 3.314 Å, and 10.478 Å, and the associated unit cell volume is 151.77 $Å^3$ [32]. In this context, the atomic structure of BP in the orthorhombic phase with space group Cmca (No. 64) is described in Fig.IV. 1 (a). Atoms are adhered by strong covalent bonds along the orbitals shaped by sp3 hybridization, creating an orthorhombic lattice with puckered honeycomb structure. The kinetic energy cutoff was 500 eV for all simulations. To attain the theoretical equilibrium crystal structure, the BP atomic structure was fully optimized with less than 0.1 eV/Å of force and 10−5 eV/atom of energy difference. A k-point mesh of 12 × 12 × 12 for the band structure calculation is adopted. Thereafter, the band structure, band gap value, dielectric response function and the refractive indices are extracted. The complex refractive index $N(\omega)=n(\omega)+ik(\omega)$ of BP with and without strain effects is then estimated from the associated dielectric function. To this extent, $n(\omega)$ denotes the refraction index and $k(\omega)$ represents the

extinction coefficient. The latter parameters are calculated by using the following equations [33]

$$k(\omega)=\frac{\left[\sqrt{\varepsilon_1(\omega)^2+\varepsilon_2(\omega)^2}-\varepsilon_1(\omega)\right]^{1/2}}{\sqrt{2}} \quad \text{(IV.1)}$$

$$n(\omega)=\frac{\left[\sqrt{\varepsilon_1(\omega)^2+\varepsilon_2(\omega)^2}+\varepsilon_1(\omega)\right]^{1/2}}{\sqrt{2}} \quad \text{(IV.2)}$$

where ε_1 and ε_2 are respectively the real and imaginary parts of the associated dielectric function.

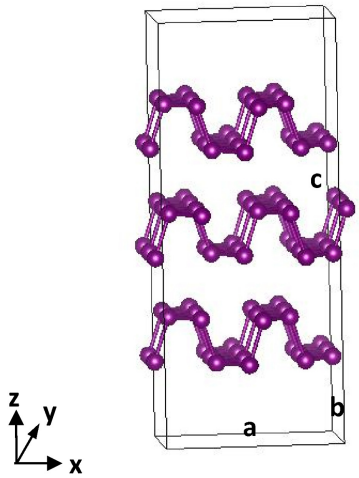

(a)

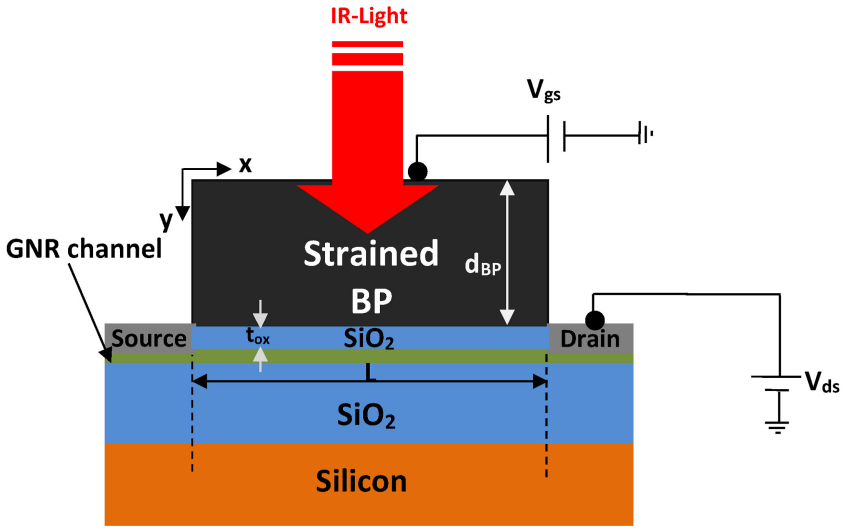

(b)

Fig. IV.1. **(a)** Orthorhombic crystal structure of bulk BP material. **(b)** Cross-sectional view of the analyzed GNR IR PT based on strained BP sensitive film.

IV.2.2 FDTD-based optical modeling of BP thin-films

The estimated optical constants of BP thin-film with and without strain effects are used to extract the absorbance (A), reflectance (R) and transmittance (T). For this purpose, the ATLAS 2-D and Luminous modules available in SILVACO software are used [34]. The latter utilizes 2-dimensional Finite-difference time-domain (2-D FDTD) to model the photogeneration mechanism BP thin-film with and without strain effects. The details of the adopted optical modeling approach can be found in [35,36]. Therefore, the optical parameters namely A and R are calculated as follows

$$A(\lambda)=\frac{\int_V \frac{1}{2}\left|\vec{E}_y(\vec{r})\right|^2 \omega\varepsilon_0\varepsilon_i''(\lambda)dV}{\int_S \frac{1}{2}\mathrm{Re}\left\{\vec{E}_y(\vec{r})\times\vec{H}^*(\vec{r})\right\}dS} \quad \text{(IV.3)}$$

$$R(\lambda)=\frac{\int_{port1}\left(E_{ci}-E_{1i}\right)E_{1i}^{*}dA_1}{\int_{port1}\left(E_{1i}E_{1i}^{*}\right)dA_1}=\frac{reflected\ power}{Incident\ power} \quad \text{(IV.4)}$$

where, λ is the wavelength, ε_0 is the permittivity of the vacuum, ε_i'' denotes the wavelength dependent complex dielectric function, which is taken from the obtained first-principles computation (Section IV.2.1) associated with bulk BP and the material under pressure. Further, E_y is the electric field in the vertical direction, $\vec{H}^*$ refers to the complex magnetic field conjugate, ω represents the angular frequency, E_{ci} is the electric field intensity at the top surface of the material and E_{1i} represents the electric field pattern of the top port.

IV.2.3 Modeling of BP-based GNR IR PT

The device structure based on combining GNR FET with strained BP IR sensitive thin-film is depicted in Fig.IV. 1 (b). The device is designed based on TFTs structure with photogating effect, involving three electrodes: gate, source and drain. The channel is suggested with 1.35 nm width and 12 atoms armchair-edge mono-layer graphene nanoribbon 2D-material, exhibiting 0.6 eV of band-gap [37]. A GNR channel length (L) with tens of nanometers is assumed, underlining the presence of quantum effects. Besides, SiO_2 oxide material with t_{ox} thickness is introduced as dielectric gate. The phototransistor operates by producing photogenerated carriers in the BP film during IR light illumination. Particularly, the amount of drain current flowing over the GNR

channel is controlled by the magnitude of the optically controlled voltage induced in the BP sensitive layer with d_{BP} of film thickness. To assess the device photoresponse properties, the phototransistor is exposed to IR-light with an optical power P_i at normal-incidence with a wavelength range of λ = [1.5 µm–10µm]. The details concerning the numerical modeling of GNR transistor by solving the Schrödinger/Poisson equations self-consistently based on non-equilibrium Green's function (*NEGF*) formalism can be found in [37,38]. In this framework, the main modeling steps are provided below.

The GNR-FET device simulation is developed based on the quantum transport numerical modeling using rigorous quantum mechanics NEGF method. The latter is considered as a highly reputed powerful tool to model nanoscale graphene based transistors with high accuracy [39,40]. Accordingly, Schrödinger equation is solved via NEGF in mode space for which the ballistic transport is considered and the charge density in GNR channel is estimated [39]. Thus, based on the Hamiltonian matrix (H) of the GNR channel [37], the retarded Green's function can expressed as follows [40].

$$G(E) = [EI - H - \Sigma_S - \Sigma_D]^{-1} \quad \text{(IV.5)}$$

where E represents the energy, I is the identity matrix, Σ_S and Σ_D are the self-energy matrices at the source and drain sides, respectively, [41,42].

The level broadening quantities ΓS and ΓD are estimated by means of the following formula [[33], [34], [35], [36]].

$$\Gamma_S = i\left(\Sigma_S - \Sigma^{+}{}_S\right) \quad \text{(IV.6-a)}$$

$$\Gamma_D = i\left(\Sigma_D - \Sigma^{+}{}_D\right) \quad \text{(IV.6-b)}$$

The local density of states resulted from the source and drain injection are calculated by using the following equations

$$D_S(E) = G\,\Gamma_S\,G^{+} \quad \text{(IV.7-a)}$$

$$D_D(E) = G\,\Gamma_D\,G^{+} \quad \text{(IV.7-b)}$$

Based on the above-mentioned formulas, the charge density in any position of the GNR channel can be calculated using the model presented in previous works [37].

$$Ne = \int_{-\infty}^{+\infty} dE \ \mathrm{sgn}[E - E_N] \times \begin{Bmatrix} D_s(E) f(\mathrm{sgn}[E - E_N](E - E_{FS})) \\ + D_D(E) f(\mathrm{sgn}[E - E_N](E - E_{FD})) \end{Bmatrix} \quad \text{(IV.8)}$$

where E_N is the partial Fermi level in armchair GNR and f is the Fermi function of the Fermi level (*EFS*).

In order to calculate the on-site electrostatic potential Ui, Finite Difference Method (FDM) is then used to solve 2D Poisson equation given by

$$\nabla^2 U = \frac{-q}{\varepsilon} \rho \quad \text{(IV.9)}$$

where U represents the electrostatic potential, ε is SiO2 dielectric constant, q denotes the electron charge and ρ is the net charge density distribution. To solve 2D Poisson equation, Neumann boundary condition is applied at the source and drain extremities, whereas at GNR/SiO2/BP contact, the Dirichlet boundary condition is exploited. Importantly, exposing the device to IR-lights can induce electron-hole pairs within the strained BP thin-film. The photo-excited carriers will be derived to the SiO2/BP interface by the applied gate voltage (Vgs), which can in turn alter the electrostatic behavior of the GNR channel. Therefore, the applied gate voltage is modified due to the generation of the photogating effects, leading to induce an effective gate voltage that can be expressed as follows

$$V_{gs}^{\ *} = V_{gs} + V_{ph}(P_i) \quad \text{(IV.10-a)}$$

$$V_{ph} = V_t \ln\left(\frac{I_{ph}}{I_s}\right) \quad \text{(IV.10-b)}$$

where V_{ph} represents the optically induced voltage [7,38], V_{gs} refers to the gate voltage and P_i is the incident IR light power, V_t is the thermal voltage, Is refers to the saturation

current and Iph is the photo-induced current density generated in the strained BP thin-film, which can be calculated by

$$I_{ph} = q\phi(1-R)\exp(-\alpha\ d_{BP}) \quad \text{(IV.11)}$$

where R is the reflection coefficient, α represents the absorption coefficient of BP material with and without strain effects, which is calculated using combined FDTD-DFT calculations presented in sections (IV.2.1) and (V.2.2), ϕ is the incident photons number expressed by $\phi = \frac{P_i}{qE_i}$, with $E_i = \frac{1.24[eV.\mu m]}{\lambda}$.

Therefore, the channel current is determined by means of the Landauer-Büttiker formula [37].

$$I = \frac{2q}{h}\int dE\, T(E)[f(E-E_{FS}) - f(E-E_{FD})] \quad \text{(IV.12-a)}$$

$$T(E) = T_r(\Gamma_S G\ \Gamma_D\ G^+) \quad \text{(IV.12-b)}$$

where *T(E)* is the transmission coefficient.

IV.3 Results and discussion

To investigate the electronic properties of bulk BP with and without strain effects, DFT calculations are performed based PBE-GGA and YS-PBE0 functionals with van der Waals (vdW) correction. In this context, the band structure is an important electronic characteristic, which can give essential information concerning the correlation between electron wave and energy vectors. This can offer the opportunity to assess the ability of BP material with and without strain effects as a building block for the design of novel optoelectronic devices. Fig.IV. 2 (a) and (b) shows respectively the electronic band structures associated with the unstrained BP thin-film and strained under pressure value of 1.2 GPa. Obviously, this figure shows that the conduction band minimum (CBM) and valence band maximum (VBM) are located at the high symmetry Z point for both material structures with and without pressure effects, indicating the direct transition nature of the band-gap. This figure demonstrates that the

introduction of strain effects can reduce the band-gap from 0.34 eV for the unstrained structure to 0.15 eV for the BP material under pressure effects (P_r = 1.2 GPa). The calculated band-gap energy value of BP thin-film using combined PBE-GGA and YS-PBE_0 functionals with van der Waals (vdW) correction (DFTD-3) is found in close agreement with the experimental results and other DFT studies employing various computation methodologies [22, 23, 24]. This proves the accurateness of the adopted computation methodology. The band-gap reduction under strain effects can be explained by the gradual overlap of p_z orbitals along the c axis when the hydrostatic pressure increases. It is worth mentioning that further increasing the hydrostatic pressure (not shown) leads to achieve closed band-gap structure (E_g = 0 eV), where CBM and VBM touch at the Z point of the first Brillouin zone. This indicates the transition from semiconductor to semimetal phase when higher pressure is considered. This phenomenon is consistent with that observed in the recent experimental investigation reported in Ref. [25]. On the other hand, the total density of states (DOS) of BP thin-film with and without strain effects is shown in Fig.IV. 2 (c). It can be seen from the latter figure that both material structures show a semiconducting nature. Moreover, the band gap is kept around the Fermi level for both strained and unstrained BP thin-films. Besides, it can be noticed from this figure that BP thin-film is free from extended states in the energy levels within the band gap, thus indicating the improved crystalline structure even when hydrostatic pressure is introduced.

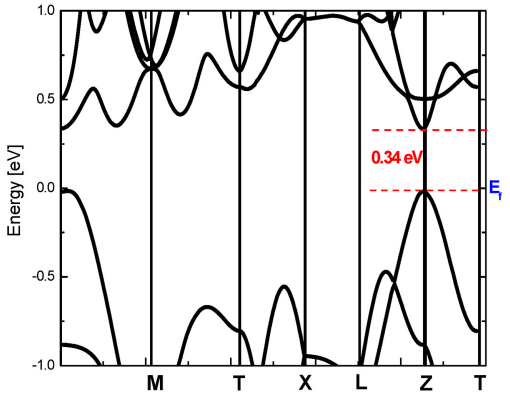

(a)

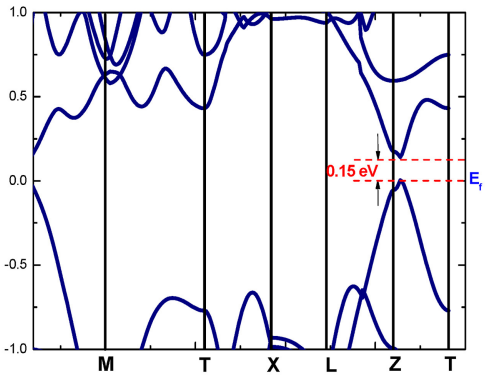

(b)

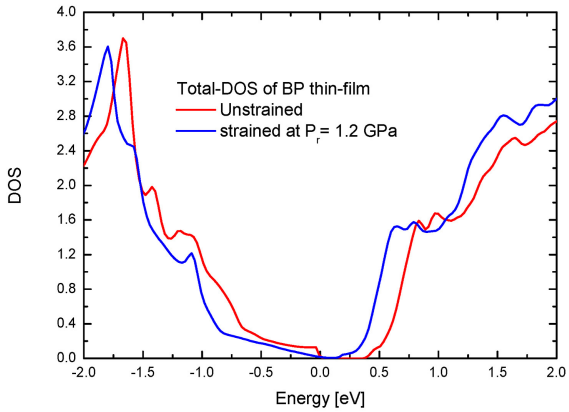

(c)

Fig. IV.2. Electronic band structure of **(a)** unstrained BP and **(b)** strained BP thin-films computed using combined PBE-GGA and YS-PBE0 functionals with DFT-D3 van der Waals correction and a pressure value of P_r = 1.2 GPa. **(c)** Density of states (DOS) of both BP materials with and without strain effects.

As a matter of fact, the analysis of the interaction between light and the material constitute an essential issue for the design of high-performance photodetection devices. To evaluate the effect of the hydrostatic pressure on the optical properties of BP thin-film, we analyze the key optical characteristics using PBE-GGA and YS-PBE_0 approaches. Accordingly, Fig.IV. 3 (a) and (b) respectively illustrate the real (ε_1) and imaginary (ε_2) parts of the dielectric function associated with BP thin-film with and without pressure effects. Obviously, this figure shows that strain effects can cause significant changes in the dielectric function of BP material. In this context, it can be observed that the strained bulk BP shows higher values of ε_1 as compared to the unstrained structure. Moreover, the maximum value of ε_2 associated with strained BP film is achieved for photon energy values around 4.3 eV, while the highest ε_2 value is reached at the specific photon energy of 4.9 eV. In addition, the static dielectric constants at zero frequency limit for both BP thin-films with and without hydrostatic pressure effects are respectively, 11.4 and 22.8. The latter values correlate well with the obtained band-gap values, where it is well-known that materials with lower band gap energy provide superior dielectric values. Furthermore, it can be observed from Fig.IV. 3 that the values of the dielectric function real part associated with strained and unstrained BP films are negative for photon energy values higher than 4.2 eV and 6 eV, respectively. This is mainly due to the metallic character of intervals of the electromagnetic spectrum. After calculating the dielectric function of both bulk BP structures with and without pressure effects, the associated absorbance spectra are extracted using 2D-FDTD method and shown in Fig.IV. 4. It is clearly shown from this figure that the strained BP film exhibits improved maximum absorbance (A = 60%) as compared to that of unstrained bulk black phosphorus (A = 38%). Moreover, by introducing pressure effects, the IR absorbance can be extended to higher wavelength values. This optical behavior is attributed to the band-gap decrease when the hydrostatic pressure is introduced as it is highlighted in the performed DFT calculations.

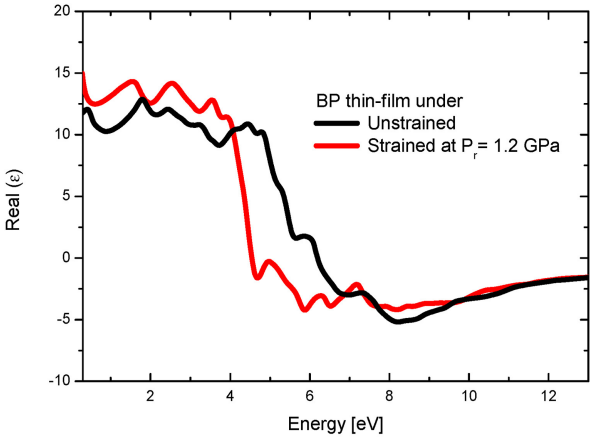

(a)

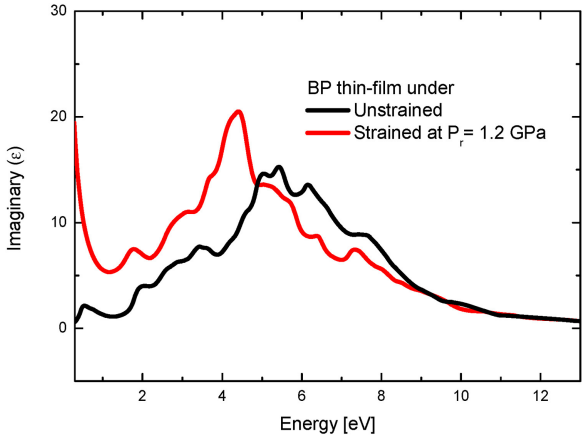

(b)

Fig. IV.3. **(a)** Real and **(a)** Imaginary parts of the dielectric function associated with BP with and without hydrostatic pressure effects obtained using DFT calculations based on PBE-GGA and YS-PBE0 functionals with DFT-D3 van der Waals correction and P_r = 1.2 GPa.

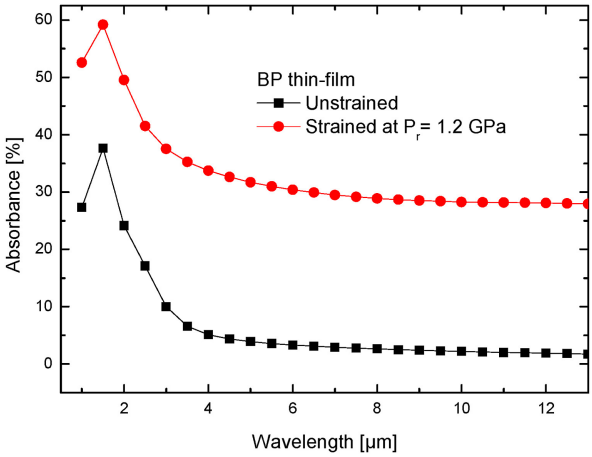

Fig. IV.4. Absorbance spectra of bulk BP thin-film with and without strain effects.

The photoresponse properties of IR–OC–GFETs are reflected by its photoconductive behavior. To elucidate and examine the influence of strain effects on the device photoconductivity, Fig.IV. 5 (a) shows the drain current versus the applied optical power at different wavelength values within the IR spectral range (λ = 3.2 µm and 8 µm) for both investigated devices based on unstrained and strained BP material with V_{gs} = 0.1 V and V_{ds} = 0.2 V. It can be observed from this figure that by increasing the IR optical power, the drain current increases for both devices. This is mainly attributed to the so-called photogating effect, where an optical voltage is generated across the BP thin sensitive film due to the photo-induced e/h pairs. The latter can be increased when the magnitude of the optical power is increased, leading to achieve the accumulation mode of the GNR-FET based transistor. This effect gives rise to an important drain-to-source current. On the other hand, Fig.IV. 5 (a) shows that the proposed IR–OC–GFET based on strained BP exhibits higher derived current capability under IR light irradiation (12 µA). The latter value is more than three orders of magnitude higher than that of the conventional GNR IR PT with unstrained BP under similar applied voltage conditions. This enhancement can be explained by the high absorption coefficient associated with strained BP material. Moreover, the phototransistor based on BP film under pressure provides a suitable photoresponse at extremely low optical powers. In other words, the proposed IR–OC–GFET requires less power to achieve a favorable photocurrent, thus underlining considerable reduction of the power consumption of the device. Fig.IV. 5 (b) illustrates the I_{ds}-V_{ds} transfer characteristics in darkness and upon light exposure at dissimilar optical power densities

of the analyzed IR–OC–GFET based on strained BP photo-gate with $\lambda = 3.2$ µm, L = 20 nm, $d_{BP} = 1$ µm, $V_{gs} = 0.1$ V, $V_{ds} = 0.1$ V and $P_r = 1.2$ GPa. This figure demonstrates the appropriate optical modulation of the channel conductivity by increasing the IR optical power intensity, where a high current under IR irradiation is reached. Basically, unlike photodiodes which have a vertical structure, the transport in the investigated IR GNR PT is carried out laterally, thus indicating the role of the channel carrier mobility in determining the derived current capability. In our case, the channel is suggested with GNR material, exhibiting very high carrier mobility. This can also explain the high drain current when the phototransistor is switched on, thus proving the merit of GNR as compared to the conventional materials. Furthermore, Fig.IV. 5 (b) shows that the proposed device offers excellent switching characteristics. This benefit is correlated with the enhanced optical control of GNR channel electrostatic behavior when strained BP film with appropriate optical characteristics is considered. To consolidate this explanation, Fig.IV. 6 (a) and (b) depict the local density of states in the GNR channel under dark and light-exposure conditions of the proposed IR–OC–GFET design based on strained BP sensitive film with $\lambda = 3.2$ µm, L = 20 nm, $V_{gs} = 0.1$ V and $P_r = 1.2$ GPa. Obviously, the band banding in the channel is modulated by illuminating the device, allowing an easy flow of current in the GNR channel when an applied drain voltage is considered. This phenomenon is explained by photogating effects, allowing the optical generation of voltage over the strained BP gate. This optical voltage acts as a gate bias and can modulate the channel electrostatic behavior by increasing the local density of states in the GNR channel.

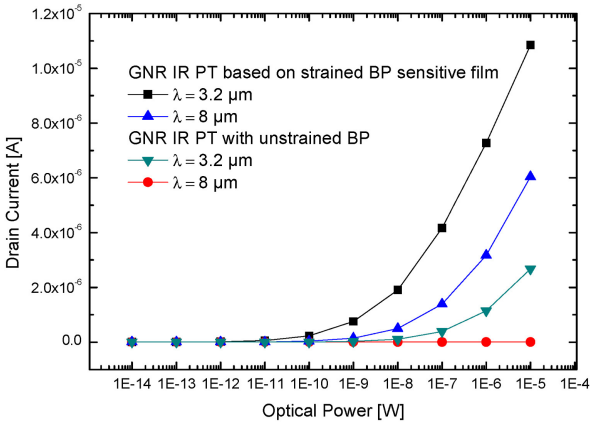

(a)

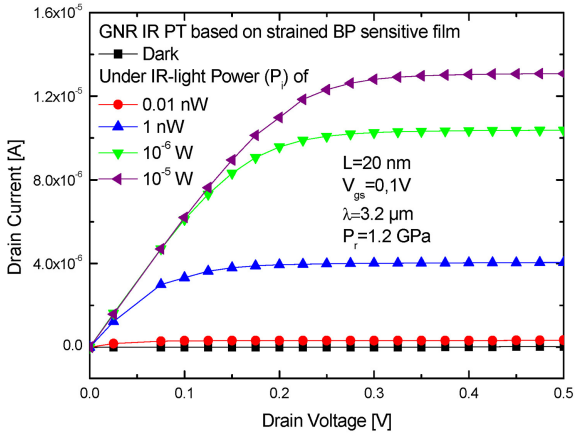

(b)

Fig. IV.5. **(a)** I-P_i characteristics of the proposed IR–OC–GFET based on BP sensitive gate with and without pressure effects illuminated at 3.2 µm and 8 µm. **(b)** I_{ds}-V_{gs} transfer characteristics of GNR IR PT based on strained BP thin-film with various optical powers, d_{BP} = 1 µm, t_{ox} = 4 nm, V_{gs} = 0.1 V, L = 20 nm and P_r = 1.2 GPa.

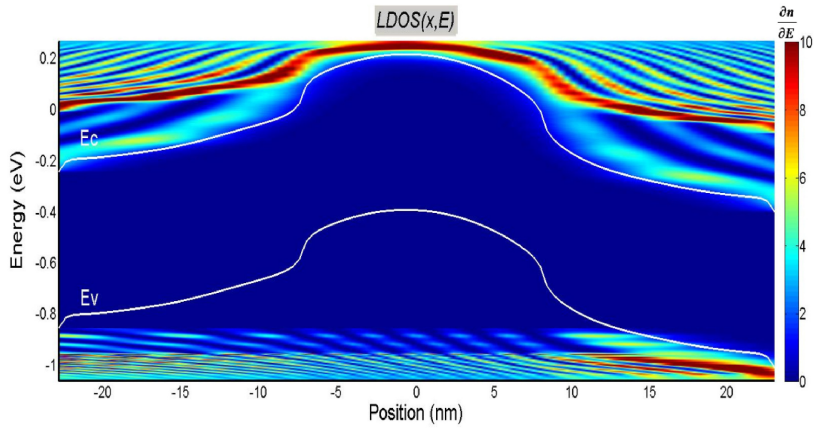

(a)

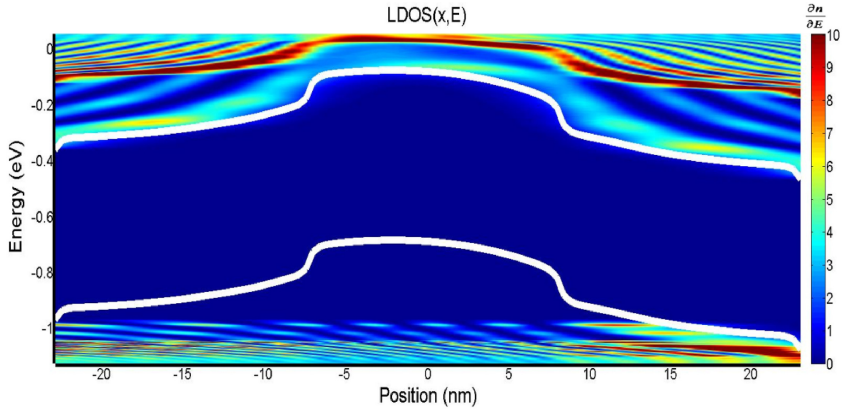

(b)

Fig. IV.6. Local density of states in GNR channel of the GNR IR PT based on strained BP photo-gate **(a)** in dark, **(b)** illuminated by IR-light at 8 µm with P_r = 1.2 GPa, t_{ox} = 4 nm, V_{gs} = 0.1 V and V_{ds} = 0.2 V.

To assess the device photoresponse performances over the IR range, the responsivity spectra of the investigated IR–OC–GFET structures based BP sensitive film with and without hydrostatic pressure are extracted and compared in Fig.IV. 7. It is clearly shown from the latter figure that the proposed phototransistor design with strained BP film exhibits superior responsivity values as compared to that of the device with unstrained BP sensitive layer. In addition, IR–OC–GFET based on unstrained BP film provides favorable responsivity over Mid-IR region; however, the device still exhibits a narrow limit in IR spectral band as it is shown in Fig.IV. 7. On the other hand, the proposed device opens up the route for achieving an extended optical sensing

band, where a high responsivity value exceeding 30 A/W is achieved over a wide spectral range of [λ = 2 µm, λ = 8.5 µm]. This proves the effectiveness of using strained BP sensitive layer for the design of broadband highly responsive IR phototransistors. The device Figure of Merits (FoMs) parameters including Responsivity, Detectivity, ION/IOFF ratio and sensitivity are computed for the investigated IR–OC–GFET designs based on BP sensitive layer with and without strain effects. The phototransistor FoM parameters are summarized in Table IV.1 and compared to recently developed IR photosensors in the literatures [43, 44, 45, 46, 47, 48, 49, 50] in order to show the strength of the proposed structure based on combined GNR channel and strained BP photo-gate paradigm. It is demonstrated from this table that the proposed phototransistor not only outperforms the conventional IR PTs in terms of device FoMs but also paves the way to achieve highly responsive sensors over a large IR spectral band. Considering these significant benefits, the proposed systematic investigation framework based on the strategic combination between first-principles calculations, FDTD optical modeling and NEGF formalism is believed to offer new insights for designing alternative high-detectivity and low power consumption IR phototransistors suitable for the emerging optoelectronic applications.

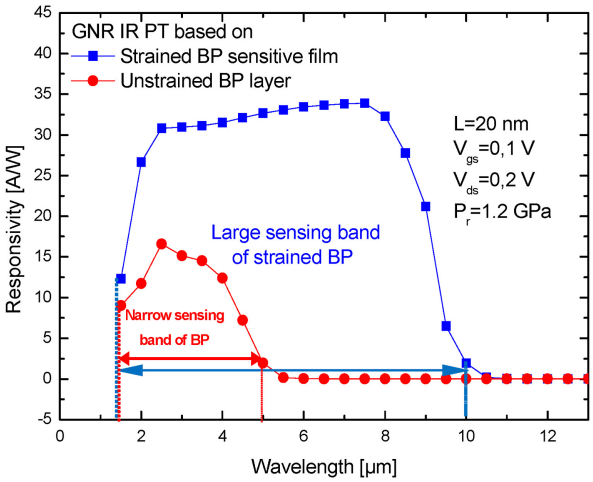

Fig. IV.7. Responsivity spectra of the investigated GNR IR PT based on BP thin-film with and without strain effects.

Table IV.1. FoMs comparison between the studied IR–OC–GFET designs based on strained BP photosensitive gate and numerous reported IR photosensors structures based on III-V and II-VI compounds, Graphene, BP-based heterostructures.

IR SENSOR DESIGNS	SENSING WAVELENGTH (µM)	I_{ON}/I_{OFF} RATIO (DB)	RESPONSIVITY (A/W)	DETECTIVITY (JONES)	SENSITIVITY	REF.
INAS/INASSB SUPERLATTICE	4.5	146	1.42	7×10^{11}	1.4×10^{4}	[215]
AL0.3GA0.7AS/GAAS HETEROINTERFACE	6.6	-	0.8	1.8×10^{10}	-	[216]
GRAPHENE/BLACK-ASP HETEROSTRUCTURE	[6-12]	-	5.8	7×10^{10}	-	[217]
GRAPHENE-Bi_2Se_3 HETEROSTRUCTURE	3.5	8.32	1.97	1.5×10^{11}	483	[218]
PHOTOCONDUCTOR BASED ON BP-ARSENIC ALLOY	[3.6-6]	-	11.2	6×10^{10}	-	[219]
BP WITH INTERDIGITATED ELECTRODES	2.5	12	0.047	-	1.8×10^{3}	[220]
BP/SiO_2/SI HETEROSTRUCTURE PT	2	-	8.5	1.7×10^{9}	-	[221]
BP/MoS_2 HETEROSTRUCTURE PHOTODIODE	3.6	53.5	0.9	1.2×10^{10}	1.3×10^{4}	[222]
GNR IR PT WITH UNSTRAINED BP FILM	3.2	57.2	15.2	7.2×10^{12}	7×10^{4}	OUR WORK
GNR IR PT WITH STRAINED BP SENSITIVE FILM	[2.2- 8]	77.8	31	1.47×10^{13}	7.8×10^{5}	OUR WORK

Finally, it seems important to provide a concept fabrication step of the proposed device. According to previously published works concerning the elaboration of GNR FET transistors [223,224], the introduced GNR channel can be fabricated by using E-beam lithography technique, where mechanically exfoliated graphene flakes from bulk graphite crystallites can be transferred to a SiO_2-coated Silicon substrate. On the other hand, the proposed sensitive gate based on BP thin-film can be deposited on the oxide/GNR structure by using Bridgman-anvil type apparatus, where powdered red phosphorus with a pressure of 9 GPa and a temperature of 673 K can be used to form BP film [51]. Subsequently, pressure effects can be introduced to realize strained BP thin-film with appropriate electronic and optical properties for IR sensing applications [52, 53].

IV.4 Conclusion

In this chapter, a systematic investigation framework based on the strategic combination between DFT computations, FDTD optical modeling and NEGF formalism is proposed to design new high-performance broadband Mid-IR-phototransistor based on strained BP sensitive gate. The impact of pressure on the electronic and optical characteristics of BP thin-film is investigated by carrying out an effective DFT calculation. The latter involves PBE-GGA and YS-PBE0 functional with DFTD3 van der Waals correction. It is found that the pressure could induce significant changes concerning the optical properties of bulk PB, where lower refractive index and band-gap energy values are achieved for the strained structure. In addition, IR–OC–GFET based on strained BP sensitive gate is modeled by self-consistently solving the Schrödinger/Poisson equations based on NEGF approach. In this context, the proposed device showcases outstanding Mid-IR photodetection properties over a broadened IR spectral range, where it yields high responsivity of 31 A/W and superior ON-to-OFF current ratio of 77 dB. Therefore, the presented systematic investigation suggests that IR phototransistors can be significantly improved by coupling graphene channel with strained BP sensitive film, opening up new perspectives for the design of alternative broadband IR photosensors for optoelectronic applications.

References

[1] A.H. Atabaki, S. Moazeni, F. Pavanello, H. Gevorgyan, J. Notaros, L. Alloatti, M. T. Wad,C. Sun, S.A. Kruger, H. Meng, K. AlQubaisi, I. Wang, B. Zhang, A. Khilo , C.V. Bai cco, M.A. Popović, V.M. Stojanović, R.J. Ram, Integrating photonics with silicon nanoelectronics for the next generation of systems on a chip, Nat. Photonics, 556 (2018), pp. 349-354

[2] J. Wei, Y. Li, L. Wang, W. Liao, B. Dong, C. Xu, C. Zhu, K.-W. Ang, C.-W. Qiu, C. Lee Zero-bias mid-infrared graphene photodetectors with bulk photoresponse and calibration-free polarization detection, Nat. Commun., 11 (2020), p. 6404

[3] M. Long, A. Gao, P. Wang, H. Xia, C. Ott, C. Pan, Y. Fu, E. Liu, X. Chen, W. Lu, T. Nilges, J. Xu, X. W, W. Hu, F. Miao, Room temperature high-detectivity mid-infrared photodetectors based on black arsenic phosphorus, Sci. Adv., 3 (2017), p. 65902

[4] C. Wang, Xi Zhang, W. Hu, Organic photodiodes and phototransistors toward infrared detection: materials, devices, and applications, Chem. Soc. Rev., 49 (2020), pp. 653-670

[5] H. Ferhati, F. Djeffal, Boosting the optical performance and commutation speed of phototransistor using SiGe/Si/Ge tunneling structure, Mater. Res. Express, 5 (2018), p. 65902

[6] S.W. Pak, D. Chu, D.Y. Song, S.K. Lee, E.K. Kim, Enhancement of near-infrared detectability from InGaZnO thin film transistor with MoS2 light absorbing layer, Nanotechnology, 28 (2017), Article 475206

[7] L. Colace, V. Sorianello, S. Rajamani, Investigation of static and dynamic characteristics of optically controlled field effect transistors, J. Lightwave Technol., 32 (2014), pp. 2233-2239

[8] D. Gola, B. Singh, P.S.T.N. Srinivas, P.K. Tiwari, Thermal noise models for tri-gate junctionless transistors including substrate bias effects, IEEE Trans. Electron. Dev., 67 (2020), pp. 263-269

[9] D. Gola, B. Singh, P.K. Tiwari, Self-heating and Negative Differential Conductance Improvement by Substrate Bias Voltage in Tri-gate Junctionless Transistor Silicon (2021)

[10] D. Gola, B. Singh, P.K. Tiwari, Subthreshold characteristic analysis and models for tri-gate SOI MOSFETs using substrate bias induced effects, IEEE Trans. Nanotechnol., 18 (2019), pp. 329-335

[11] D. Gola, B. Singh, J. Singh, S. Jit, P.K. Tiwari, Static and quasi-static drain current modeling of tri-gate junctionless transistor with substrate bias induced effects, IEEE Trans. Electron. Dev., 66 (2019), pp. 2876-2883

[12] H. Ferhati, F. Djeffal, A new high-performance phototransistor design based on both surface texturization and graded gate doping engineering, J. Comput. Electron., 15 (2016), pp. 301-310

[13] H. Ferhati, F. Djeffal, Planar Junctionless Phototransistor: A Potential High-Performance and Low-Cost Device for Optical-Communications, vol. 97, Optics & Laser Technology (2017), p. 29

[14] T. Bentrcia, F. Djeffal, A. Benhaya, Continuous analytic I-V model for GS DG MOSFETs including hot-carrier degradation effects, J. Semiconduct., 33 (2012), p. 14001

[15] A.K. Geim, K.S. Novoselov, The rise of grapheme, Nat. Mater., 6 (2007), pp. 183-191

[16] Y.-W. Son, M.L. Cohen, S.G. Louie, Energy gaps in graphene nanoribbons, Phys. Rev. Lett., 97 (2006), 216803-1–216803-4

[17] X. Liu, X. Ji, M. Liu, N. Liu, Z. Tao, Q. Dai, L. Wei, C. Li, X. Zhang, B. Wang, High-performance Ge quantum dot decorated graphene/zinc-oxide heterostructure infrared photodetector, ACS Appl. Mater. Interfaces, 7 (2015), pp. 2452-2458

[18] Z. Pei, H. Lai, J. Wang, W. Chiang, C. Chen, High-responsivity and high-sensitivity graphene dots/a-IGZO thin-film phototransistor, IEEE Electron. Device Lett., 36 (2015), pp. 44-46

[19] Z. Pei, H. Lai, J. Wang, W. Chiang, C. Chen, High-responsivity and high-sensitivity graphene dots/a-IGZO thin-film phototransistor, IEEE Electron. Device Lett., 36 (2015), pp. 44-46

[20] J. Cheng, C. Wang, X. Zou, L. Liao, Recent advances in optoelectronic devices based on 2D materials and their heterostructures, Adv. Opt. Mater., 7 (2018), Article 1800441

[21] C. Xie, Y. Wang, Z.-X. Zhang, D. Wang, L.-B. Luo, Graphene/semiconductor hybrid heterostructures for optoelectronic device applications, Nano Today, 19 (2018), pp. 41-83

[22] L. Li, Y. Yu, G.J. Ye, Q. Ge, X. Ou, H. Wu, D. Feng, X.H. Chen, Y. Zhang, Black phosphorus field-effect transistors, Nat. Nanotechnol., 9 (2014), pp. 372-377

[23] J. Qiao, X. Kong, Z.-X. Hu, F. Yang, W. Ji, Few-layer black phosphorus: emerging 2D semiconductor with high anisotropic carrier mobility and linear dichroism, Nat. Commun., 5 (2014), p. 4475

[24] L. Huang, K.-W. Ang, Black phosphorus photonics toward on-chip applications, Appl. Phys. Rev., 7 (2020), p. 31302

[25] Z.J. Xiang, G.J. Ye, C. Shang, B. Lei, N.Z. Wang, K.S. Yang, D.Y. Liu, F.B. Me ng, X.G. Luo, L.J. Zou, Z. Sun, Y. Zhang, X.H. Chen, Pressure-induced electronic transition in black phosphorus, Phys. Rev. Lett., 115 (2015), Article 186403

[26] S.E. Farah, Z. Dibi, H. Ferhati, F. Djeffal, DFT-FDTD modeling of a new broadband mid-infrared IGZO thin-film phototransistor based on black phosphorus capping layer incorporating intermediate metallic film, J. Phys. Chem. Solid., 162 (2022), Article 110528

[27] P. Perdew, K. Burke, M. Ernzerhof, Generalized gradient approximation made simple Phys. Rev. Lett., 77 (1996), p. 3865
[28] F. Tran, P. Blaha, Implementation of screened hybrid functionals based on the Yukawa potential within the LAPW basis set,Phys. Rev. B, 83 (2011), Article 235118
[29] L.B. Drissi, F.Z. Ramadan, H. Ferhati, F. Djeffal, N.B.-J. Kanga, New highly efficient 2D SiC UV-absorbing material with plasmonic light trapping, J. Phys. Condens. Matter, 32 (2019), p. 25701
[30] J. Heyd, G.E. Scuseria, Efficient hybrid density functional calculations in solids: assessment of the Heyd–Scuseria–Ernzerhof screened Coulomb hybrid functional, J. Chem. Phys., 121 (2004), pp. 1187-1192
[31] S. Grimme, J. Antony, S. Ehrlich, H. Krieg, A consistent and accurate ab initio parametrization of density functional dispersion correction (DFT-D) for the 94 elements H-Pu, J. Chem. Phys., 132 (2010), Article 154104
[32] R. Wyckoff, Crystal Structures, John Wiley, New York (1963)
[33] F. Elhamra, S. Lakel, H. Meradji, Pressure effect on the structural, electronic, optical and elastic properties of Zn0.75Be0.25O from first-principles calculations, Optik, 15 (2019), pp. 115-138
[34] Atlas User's manual, SILVACO TCAD, (2012)
[35] H. Ferhati, F. Djeffal, Role of optimized grooves surface -textured front glass in improving TiO2 thin film UV photodetector performance, IEEE Sensor. J., 16 (2016), pp. 5618-5624
[36] F. Srairi, F. Djeffal, H. Ferhati, Efficiency increase of hybrid organic/inorganic solar cells with optimized interface grating morphology for improved light trapping, Optik, 130 (2017), pp. 1092-1098
[37] K. Tamersit, F. Djeffal, Double-gate graphene nanoribbon field-effect transistor for DNA and gas sensing applications: simulation study and sensitivity analysis, IEEE Sensor. J., 16 (2016), pp. 4180-4191
[38] A. Kadri, H. Ferhati, F. Djeffal, Giant responsivity of a new optically controlled graphene UV-phototransistor using graded band-gap ZnMgO gate, Sensor Actuator Phys., 325 (2021), Article 112701
[39] G. Fiori, G. Iannaccone, Multiscale modeling for graphene-based nanoscale transistors, Proc. IEEE, 101 (2013), pp. 1653-1669
[40] A.Martinez, M. Bescond, J.R. Barker, A. Svizhenko, M.P. Anantram, C. Millar, A. Asenov, A self-consistent full 3-D real-space NEGF simulator for studying nonperturbative effects in nano-MOSFETs, IEEE Trans. Electron. Dev., 4 (2007), pp. 2213-2222
[41] P. Zhao, J. Guo, Modeling edge effects in graphene nanoribbon field-effect transistors with real and mode space methods, J. Appl. Phys., 105 (2009), p. 34503
[42] K. Tamersit, F. Djeffal, A novel graphene field-effect transistor for radiation sensing application with improved sensitivity: proposal and analysis, Nucl.

Instrum. Methods Phys. Res. Sect. A Accel. Spectrom. Detect. Assoc. Equip., 901 (2018), pp. 32-39

[43] D. Wu, J. Li, A. Dehzangi, M. Razeghi, High performance InAs/InAsSb Type-II superlattice mid-wavelength infrared photodetectors with double barrier, Infrared Phys. Technol., 109 (2020), Article 103439

[44] T. Murata, S. Asahi, S. Sanguinetti, T. Kita, Infrared photodetector sensitized by InAs quantum dots embedded near an Al0.3Ga0.7As/GaAs heterointerface, Sci. Rep., 10 (2020), p. 11628

[45] V. Ryzhii, M. Ryzhii, V. Mitin, M.S. Shur, T. Otsuji,Far-infrared photodetectors based on graphene/black-AsP heterostructures, Opt Express, 28 (2020), pp. 2480-2498

[46] M. Ye, J. Zha, C. Tan, K.B. Crozier, Highly sensitive, gate-tunable, room-temperature mid-infrared photodetection based on Graphene−Bi2Se3 heterostructure, Appl. Phys. Rev., 8 (2021), p. 31303

[47] M. Amani, E. Regan, J. Bullock, G.H. Ahn, A. Javey, Mid-wave infrared photoconductors based on black phosphorus-arsenic alloys, ACS Nano, 11 (2017), pp. 11724-11731

[48] M. Xu, Y. Gu, R. Peng, N. Youngblood, M. Li, Black phosphorus mid-infrared photodetectors, Appl. Phys. B, 123 (2017), pp. 123-130

[49] L. Huang, W.C. Tan, L. Wang, B. Dong, C. Lee, K.-W. Ang, Infrared black phosphorus phototransistor with tunable responsivity and low noise equivalent power, ACS Appl. Mater. Interfaces, 41 (2017), pp. 36130-36136

[50] J. Bullock, M. Amani, J. Cho, Y.Z. Chen, G.H. Ahn, V. Adinolfi, V.R. Shrestha, Y. Gao, K.B. Crozier, Y.-L. Chueh, A. Javey, Polarization-resolved black phosphorus/molybdenum disulfide mid-wave infrared photodiodes with high detectivity at room temperature, Nat. Photonics, 12 (2018), pp. 601-607

[51] W. Xu, T.-W. Lee, Recent progress in fabrication techniques of graphene nanoribbons, Materials Horizons, 3 (2016), p. 186

[52] M. Evaldsson, I.V. Zozoulenko, Hengyi Xu, T. Heinzel, Edge-disorder-induced Anderson localization and conduction gap in graphene nanoribbons, Phys. Rev. B, 78 (2008), p. 161407

[53] T. Kikegawa, H. Iwasaki, Edge-disorder-induced Anderson localization and conduction gap in graphene nanoribbons, Acta Crystallogr., 39 (1983), pp. 158-164

[54] S. E. Farah, F. Dieffal, Z. Dibi and H. Ferhati, "Electrical and optical properties of Black Phosphorus under Strain effects: A First-principles Study," 2022 19th International Multi-Conference on Systems, Signals & Devices (SSD), Sétif, Algeria, 2022, pp. 236-241, doi: 10.1109/SSD54932.2022.9955983.

Conclusion

1. Conclusion

The various threads of this thesis are all focused on the design, modeling, and optimization of new BP-based optoelectronic devices. Moreover, this thesis has explored various aspects for enhancing BP-based phototransistors. This is motivated primarily by the sense that enhancing the IR photoresponse, reducing the power consumption and enlarging the spectral band of the IR sensor is highly valuable for developing high-performance optoelectronic systems. This dissertation develops several design methodologies and optimization frameworks to address the challenges associated with the emerging IR sensors. The thesis is composed of four subsequent sections

First, we presented an summary of the state-of-the-art research in phosphorene taking into account the crystal structure, physical and chemical properties, synthesis methods, advances and several applications... Several of the outstanding properties, advances and applications of phosphorene, are emphasized. This chapter also summarized recent progress in phosphorene and its future directions. The peculiar structure of BP and phosphorene sets its apart from graphene and other largely studied 2D semiconductors.

Thereafter, we described the Density Functional Theory (DFT) which is a powerful method and often used quantum mechanical instrument for examining different features of matter. Designing and evolving more effective density functionals is a constant process since there are still problems to be solved, and it is a quantum fantasy to get all the qualities right at an affordable computational cost.

Afterward, a novel broadband mid-IR IGZO TF PT based on both Black Phosphorus capping layer incorporating intermediate gold ultrathin-film is proposed. The optical and electronic properties of the Black Phosphorus are carried out using DFT computations that include PBE-GGA and YS-PBE0 functionals with DFT-D3 van der Waals correction. The absorbance of the BP sensing layer including intermediate gold ultra-thin film is performed using FDTD-based numerical modeling frameworks. To boost up the absorbance performance of the BP/Au/BP sensing layer, we combined FDTD modeling and PSO optimization technique which permits achieving near-perfect broadband mid-IR absorbance behavior. It is found that the optimized BP/Au/BP capping film can extend the device photoresponse within the mid-IR spectral range,

offering a high current ratio, high responsivity and superior detectivity of over a wide operating voltage window. Considering these significant performances, the proposed approach is expected to provide a valuable guideline for the development of highly sensitive broadband photosensors.

Finally, a systematic investigation framework based on the strategic combination between DFT computations, FDTD optical modeling and NEGF formalism is proposed to design new high-performance broadband Mid-IR-phototransistor based on strained BP sensitive gate. The impact of pressure on the electronic and optical characteristics of BP thin-film is investigated by carrying out an effective DFT calculation. The latter involves PBE-GGA and YS-PBE0 functional with DFTD3 van der Waals correction. It is found that the pressure could induce significant changes concerning the optical properties of bulk PB, where lower refractive index and band-gap energy values are achieved for the strained structure. In addition, IR–OC–GFET based on strained BP sensitive gate is modeled by self-consistently solving the Schrödinger/Poisson equations based on NEGF approach. In this context, the proposed device showcases outstanding Mid-IR photodetection properties over a broadened IR spectral range, where it yields high responsivity and superior ON-to-OFF current ratio. Therefore, the presented systematic investigation suggests that IR phototransistors can be significantly improved by coupling graphene channel with strained BP sensitive film, opening up new perspectives for the design of alternative broadband IR photosensors for optoelectronic applications.

We believe that the dissertation represents a significant contribution to the field of IR optoelectronic systems. In light of these noteworthy results, it is anticipated that the suggested methodology will offer a useful framework for the advancement of extremely sensitive broadband photosensors.

2. Outlooks

The versatility of the dissertation work can contribute considerably to basic understanding of various novel IR sensors. The obtained results regarding the development of alternative BP-based IR phototransistors could be useful for researchers to develop new pathways for further enhancing the device performance. In this framework, the development of more advanced IR-sensors seems to be interesting which would take into account other aspects such as the time response, IR

photoresponse, the manufacturing cost and further reduce concerning the power budget. Thus, the present work can be extended by considering the following topics, which highlight the possible future directions for further development of high-performance optoelectronic devices.

First, the elaboration and characterization of the optimized IGZO TF PT based on BP/Au/BP capping film. Moreover, the exploration of new possibilities to incorporate plasmonic nanoparticles using various metals for further extending the IR spectral photoresponse. Besides, exploring the possibility of using few layers of BP material as a sensitive film seems interesting. This can potentially modulate the device detection properties. Second, the use of DFT computation to explore new IR sensitive materials, offering improved electronic, optical and electrical properties for broadband IR detection applications.